High-frequency internal waves on a sloping shelf

James M. Pringle[1] and Kenneth H. Brink

Woods Hole Oceanographic Institution, Woods Hole, Massachusetts, 02543

Abstract. The behavior of an internal wave in a continuously stratified fluid over a sloping bottom is examined by finding approximate analytic solutions for the amplitude of waves in a coastal ocean with constant bottom slope, linear bottom friction, and barotropic mean flows. These solutions are valid for frequencies higher than the frequency of critical reflection from the sloping bottom. The solutions show that internal waves propagating toward the shore are refracted, so that their crests become parallel to shore as they approach the coast, and outward propagating waves are reflected back toward the coast from a caustic. Inviscid solutions predict that the amplitude of a wave goes to infinity at the coast, but these infinite amplitudes are removed by even infinitesimal bottom friction. These solutions for individual rays are then integrated for an ensemble of internal wave rays of random orientation that originate at the shelf break and propagate across the shelf. It is found that for much of the shelf the shape of the current ellipse caused by these waves is nearly independent of the waves' frequency. The orientation of the current ellipse relative to isobaths is controlled by the redness of the internal wave spectrum at the shelf break and the strength of mean currents. Friction is more important on broader shelves, and consequently, on broad shelves the internal wave climate is likely to be dominated by any internal waves generated on the shelf, not waves propagating in from the deep ocean.

1. Introduction

An internal wave propagating obliquely into a coast will turn into the coast, so that its crests will become more parallel to the shore as it moves inward. A wave propagating obliquely offshore will turn so that its crests become more perpendicular to the shore. This effect, noted by *Wunsch* [1969] and *McKee* [1973], will modify the directional spectra of an internal wave field propagating across a shelf and hence control the high-frequency variability on the shelf. This analysis examines the evolution of the high-frequency internal wave field on the shelf as it is modified by this refraction, mean barotropic currents, and bottom friction.

The study of the cross-shelf evolution of the internal wave field is begun by finding a solution for the amplitude of a progressive, linear, internal wave crossing a wedge-shaped bathymetry obliquely in the presence of linear bottom friction and barotropic mean alongshore currents. These solutions extend the results of *McKee* [1973], who gave the first correct solution for an internal wave obliquely crossing an inviscid, quiescent, wedge-shaped shelf, and *Wunsch* [1969], who described a progressive internal wave crossing a wedge-

shaped shelf normal to the coast. Like the solutions of *McKee* [1973], the solutions derived herein are limited to frequencies higher than that of critical reflection from the bathymetry.

The solutions for the propagation of individual internal waves across the shelf are then used to model the evolution of an ensemble of internal waves propagating across the shelf. This is an important and useful exercise because the currents driven by the ensemble of internal waves can differ markedly from the currents driven by a single internal wave, and thus predicting the observations of a current meter or the response of an organism to the internal wave field from the characteristic of a single plane wave can be deceptive. The ensemble is chosen to resemble the *Garrett and Munk* [1972] spectrum at a distance offshore chosen to represent the shelf break. It is clearly naive to assume that the spectrum at the shelf break is a Garrett and Munk spectrum, nevertheless, observations at the shelf break and over the shelf find that the Garrett and Munk spectrum is not a very bad approximation of the internal wave climate near the shelf break [*Pringle*, this issue]. More detailed modeling of the propagation of internal waves across a shelf break in the limit of a steep shelf break is given by *Chapman and Hendershott* [1981].

This analysis does not model the effect on internal waves of a baroclinic mean flow, nor does it attempt to explain the nonlinear evolution of nearly linear waves due to wave-wave interactions as the waves move onshore. It also ignores the possible effects of alongshore variation in the mean flow and bathymetry. These are quite possibly important effects and deserve further attention. Nevertheless, the solutions derived below could be used as the basis functions for scattering solutions to weakly interacting nonlinear problems and the small baroclinic shear problem. The solutions are used to indicate what scales of alongshore variation are important. Because the present analysis does not model the evolution of a wave moving over a topography whose bottom slope is the same as or greater than that needed for critical reflection from the bottom, the following analysis is not valid for near-inertial waves. (For a bottom slope of 5×10^{-3}, the frequency must be at least 5% greater than the inertial frequency f for a bouyancy frequency N of 100 cpd). In a companion paper [*Pringle*, this issue], the high-frequency internal waves observed off the coast of California, United States, as part of the 1982 Coastal Ocean Dynamics Experiment (CODE), are analyzed.

2. Plane Internal Wave Solution

In a flat bottom ocean the internal wave spectrum can be broken into vertical modes that are orthogonal to each other [*LeBlond and Mysak*, 1978]. Defining u and v as horizontal velocities and w as vertical velocity, the linearized inviscid system of equations on an f plane is

$$\begin{aligned}
\frac{\partial u}{\partial t} - fv &= -\frac{1}{\rho_0}\frac{\partial P}{\partial x}, && \text{(1a)}\\
\frac{\partial v}{\partial t} + fu &= -\frac{1}{\rho_0}\frac{\partial P}{\partial y}, && \text{(1b)}\\
\frac{\partial w}{\partial t} &= -\frac{1}{\rho_0}\frac{\partial P}{\partial z} - \frac{\rho g}{\rho_0}, && \text{(1c)}\\
\frac{\partial u}{\partial x} + \frac{\partial v}{\partial y} + \frac{\partial w}{\partial z} &= 0, && \text{(1d)}\\
\frac{\partial \rho}{\partial t} - \frac{\rho_0}{g}N^2(z)w &= 0. && \text{(1e)}
\end{aligned}$$

N is buoyancy frequency, P is pressure, g is local gravitational acceleration, f is Coriolis frequency, ρ_0 is mean water density, and ρ the local deviation of density from ρ_0. The coordinate system is right-handed with z positive upward. Where the bottom is flat, this system admits internal wave solutions of the form

$$\begin{aligned}
u &= \Re\left[\frac{i\omega k - fl}{\omega\left(k^2+l^2\right)}\frac{dW}{dz}e^{i(kx+ly-\omega t)}\right] && \text{(2a)}\\
v &= \Re\left[\frac{i\omega l + fk}{\omega\left(k^2+l^2\right)}\frac{dW}{dz}e^{i(kx+ly-\omega t)}\right] && \text{(2b)}\\
w &= \Re\left[W(z)e^{i(kx+ly-\omega t)}\right] && \text{(2c)}
\end{aligned}$$

where ϕ is an arbitrary phase, k is the horizontal wave number, ω is the angular frequency, and $W(z)$ is the vertical modal structure. $W(z)$ and k are determined for a given ω by

$$\frac{d^2W}{dz^2} + \left(k^2+l^2\right)\left[\frac{N^2(z)-\omega^2}{\omega^2-f^2}\right]W = 0 \qquad (3)$$

with $W = 0$ at the surface and bottom. If N is independent of depth, W has the form

$$W = \sin\left(\frac{M\pi}{D}z\right) \qquad M = 1...\infty, \qquad (4)$$

where D is the water depth and M is the mode number. When N varies with depth, (3) must usually be solved numerically and the profile is no longer independent of ω. Nonetheless, the structure does not vary strongly with changes in ω or in the N profile as long

as $\omega^2 \ll N^2$. This is because any change in

$$\frac{N^2(z) - \omega^2}{\omega^2 - f^2} \tag{5}$$

only affects the solution to the extent that (5) varies from its depth-averaged value. Any constant multiplicative change to its value is absorbed into the eigenvalue $k^2 + l^2$ and does not affect $W(z)$. To illustrate this, the first vertical mode is plotted in Figure 1 for two different frequencies, 2 and 40 cpd, and two different stratifications, a constant N and an N that varies realistically from 100 cpd at the surface to 50 cpd at the bottom. The depth-varying stratification, shown in Figure 2, is derived from the mean density structure computed in the Coastal Ocean Dynamics Experiment region during July 1982 from conductivity-temperature-depth (CTD) and current meter data [*Pringle*, this issue]. Neither changes in frequency nor the depth-dependent N affects the modal structure very much. Because of this, there are only small differences between the dispersion relation for a constant N and the dispersion relation for a variable N, as long as $\omega^2 \ll N^2$. Thus the following work should only be applied to internal waves satisfying $\omega^2 \ll N^2$, and the depth-averaged N should be used for stratification in comparing this work with observations.

Figure 1

Figure 2

The modal solutions suppose a flat bottom in their bottom boundary condition. The boundary condition for a sloping bottom is that the velocity normal to the boundary be zero. *Wunsch* [1969] shows that the solution over a wedge-shaped topography limits to the flat bottom result when the slope of the wave characteristics c,

$$c = \sqrt{\frac{\omega^2 - f^2}{N^2 - \omega^2}}, \tag{6}$$

becomes more then twice the bottom slope α. (This can be most easily seen by directly comparing equations (8) and (12) of *Wunsch* [1969]. The error in using the flat bottom modal solution is less than 10% when $0.5c > \alpha$.) The criterion for the validity of using vertical modes can thus be obtained by solving (6) for frequency and substituting twice the bottom slope for the characteristic wave slope, leading to

$$\omega^2 > f^2 + 4\alpha^2 N^2. \tag{7}$$

For an f of 1.24 cpd and an N of 100 cpd, this is true for frequencies 28% higher than f for a slope of 5×10^{-3} and 90% higher than f for a slope of 10^{-2}. This frequency criterion is equivalently the condition for avoiding critical reflection off the bottom, thus any

wave whose vertical structure is well described by (3) is not subject to critical reflection from the bottom. The relation between these two facts is explored by *Wunsch* [1969].

3. Path of a Wave With No Mean Flow

The first step in understanding the propagation of internal waves on the shelf is to study the behavior of a single plane wave on a shelf with no mean flow, constant N, and no alongshore variability in topography.

Basic ray-tracing theory [*Lighthill*, 1978] states that if there is no variation in the alongshore direction, the alongshore wave number l is conserved along a ray, and if there is no variation with time, the observed frequency ω is conserved along a ray. From (3) the dispersion relation for the modal internal waves in the absence of mean flow is

$$\omega = \sqrt{\frac{(k^2 + l_0^2)N^2 + f^2\frac{M^2\pi^2}{D^2}}{k^2 + l_0^2 + \frac{M^2\pi^2}{D^2}}}, \tag{8}$$

where l_0 is the conserved alongshore wave number. Given a depth D_0 and a cross-shelf wave number k_0 at any point on the ray path, one can find the cross-shelf wavenumber k_m at any other point on the ray path where one knows the depth D_m

$$k_m^2 = \frac{D_0^2}{D_m^2}(k_0^2 + l_0^2) - l_0^2. \tag{9}$$

Because the internal wave dispersion relation (8) depends only on the horizontal wave vector magnitude, not its direction, the group velocity $\mathbf{c_g}$ is parallel to the wave vector. Since the group velocity is parallel to the wave vector and since the group velocity defines the ray path, the equation of the ray path is

$$\frac{dy}{dx} = \frac{dy/dt}{dx/dt} = \frac{\mathbf{c_g}\cdot\hat{j}}{\mathbf{c_g}\cdot\hat{i}} = \frac{l}{k}. \tag{10}$$

To find the path of a wave, a specific bathymetry, $D(x)$, must be specified. For the sake of simplicity a linear, wedge-shaped topography is chosen, with the coast at $x = 0$ and the sea extending to $x = -\infty$. The depth is $D = -\alpha x$. None of the results below is qualitatively affected by the choice of depth profile, as long as the bottom slope remains finite as one approaches the shore. Equation (9) can be substituted for k and (10) integrated to get the ray path

$$y = \pm x_c\sqrt{1 - \frac{x^2}{x_c^2}}, \tag{11}$$

where, from (8) and the definition of the depth,

$$x_c = \frac{M\pi c}{\alpha l_0}. \tag{12}$$

This path is a half circle whose radius is x_c. The ray path in (11) defines the path along which the internal wave energy will propagate, in either direction, as long as ray tracing remains valid. As shown in the appendix, ray tracing remains valid, except near x_c where

$$\frac{(x + x_c)}{x_c} \leq 2^{-\frac{1}{3}} \left(\frac{M\pi c}{\alpha} \right)^{-\frac{2}{3}}. \tag{13}$$

Since $c\alpha^{-1}$ must be much greater than 1 for vertical modes to exist, the region where ray tracing fails is a small portion of the region inshore of $-x_c$. For a mode 1 wave with $\omega = 10$ cpd, $N = 100$ cpd, f=1.24 cpd, and a bottom slope of 5×10^{-3}, ray tracing is valid for 95% of the distance between the shore and $-x_c$. There is a caustic at $-x_c$, and the energy in the wave is reflected back to the coast from this region, trapping the wave inshore of $-x_c$. The only way a wave with $l \neq 0$ can travel farther offshore than x_c is for the vertical modal structure to break down or for the mode to "stop feeling" the bottom. The vertical mode assumption can break down if the bottom slope exceeds the critical value in (6). Alternatively, the vertical mode can cease to feel the bottom and hence cease to be steered by the topography if the stratification N near the bottom falls below ω. Likewise, waves propagating onshore from the deep ocean will only begin to be governed by (11) when $N > \omega$ near the bottom and the bottom slope is less than the critical slope.

The derivation above assumes that there is no alongshore variation in the bathymetry. Equation (11) shows that a wave trapped inside of $x = -x_c$ will travel a distance of $2x_c$ along the coast before the ray intersects the coast. This implies that alongshore variation has to be small over a distance of $2x_c$ for these derivations to be valid. Thus a shelf can be considered uniform in the along-shelf direction if the bathymetry and mean currents do not vary over an alongshore distance comparable to the distance between the shelf break and the shore.

4. Wave Amplitude With No Mean Flow

A wave traveling in the absence of a mean current carries energy along its ray path at the speed of the group velocity $\mathbf{c_g}$. [*Lighthill*, 1978, p. 321]. This means

that the conservation of the areal energy density can be expressed as

$$\nabla \cdot (\mathbf{c_g} E) = T^{-1} E \tag{14}$$

where T is the timescale of the dissipation of wave energy by friction. It is easier to work with the depth-averaged volume energy density $\langle E_d \rangle$ of the wave

$$\langle E_d \rangle = \frac{1}{4} \rho_0 A_h^2 \left(\frac{N^2 - f^2}{N^2 - \omega^2} \right) = \frac{W_0^2 \rho_0 N^2}{4\omega^2}, \tag{15}$$

where W_0 is the amplitude of the vertical velocity mode (3c) and A_h is the amplitude of the horizontal velocity mode (3a). Using the depth-averaged volume energy density, (14) becomes

$$\nabla \cdot (\mathbf{c_g} D \langle E_d \rangle) = T^{-1} D \langle E_d \rangle. \tag{16}$$

where D is the water depth. Since there is no variation in the alongshore direction, (16) can be written as

$$\frac{\partial}{\partial x} \left(\hat{i} \cdot \mathbf{c_g} D \langle E_d \rangle \right) = T^{-1} D \langle E_d \rangle. \tag{17}$$

The cross-shelf component of the group velocity, $\hat{i} \cdot \mathbf{c_g}$, can be written as

$$\hat{i} \cdot \mathbf{c_g} = |\mathbf{c_g}| \, \frac{k}{\sqrt{k^2 + l^2}} \tag{18}$$

because the wave vector is parallel to the group velocity. The magnitude of the group velocity, $|\mathbf{c_g}|$, can be found by taking the wave number derivative of (8) and using (9) to find the local k in terms of the water depth D. This yields

$$|\mathbf{c_g}| = SD, \tag{19a}$$

$$S = \frac{c(N^2 - f^2)}{M\pi(1 + c^2)^{\frac{3}{2}}(c^2 N^2 + f^2)^{\frac{1}{2}}}, \tag{19b}$$

where S is a constant with units of time^{-1} and c is the characteristic internal wave slope defined by (6).

The dissipation timescale T can be estimated from a frictional analysis based on *Brink* [1988] and extended to high-frequency internal waves over a sloping bottom in the appendix. The analysis assumes a linear bottom drag law

$$\tau_{\text{bottom}} = \rho_0 r \mathbf{u}_{\text{bottom}}, \tag{20}$$

and that this friction is weak, i.e., that the timescale of the friction, Dr^{-1}, is much greater then the timescale of the wave ω^{-1}. This restriction remains valid for a reasonable value of r, $r = 5 \times 10^{-4}$ m s^{-1}, and ω, 10 cpd,

until the water is only 5m deep. A comparison of more complicated drag laws with the linear law is given by *Sanford and Grant* [1987]. *Brink* [1988] shows that the energy density of a plane wave in constant stratification over a flat bottom decays as

$$\langle E_d \rangle = \langle E_d \rangle_0 \exp\left[-2\frac{r}{D}\left(1+\frac{f^2}{\omega^2}\right)t\right], \tag{21}$$

and so timescale of energy decay T will be approximated here as

$$T = \frac{D}{2r}\left[1+O\left(\frac{f^2}{\omega^2}\right)\right]. \tag{22}$$

The frictional timescale (22), the cross-shelf component of the group velocity (18), and the depth $D=-\alpha x$ can now be used to write the equation for the cross-shelf evolution of $\langle E_d \rangle$, (16), as

$$\frac{\partial}{\partial x}\left(x^2\sqrt{1-\frac{x^2}{x_c^2}}\langle E_d\rangle\right) = \pm\frac{2r}{S\alpha^2}\langle E_d\rangle. \tag{23}$$

The right-hand side is positive when the wave is propagating offshore and negative when the wave is propagating toward the coast. If there is no bottom friction, i.e. $r=0$, (23) can be solved to obtain

$$\langle E_d \rangle = \frac{\mathcal{C}}{x^2\sqrt{1-\frac{x^2}{x_c^2}}}, \tag{24}$$

where $\mathcal{C}$ is a constant.

From (24) it can be seen that as $x \to 0$, $\langle E_d \rangle$ grows as x^{-2}. This amplification has two causes. First, as the water depth decreases, the volume energy density for a given areal energy density increases as D^{-1} and so x^{-1}. Second, from (19) the magnitude of the group velocity decreases linearly as depth decreases, and so the areal energy density also has to increase as D^{-1} and x^{-1} to keep the energy flux constant.

However, even the smallest amount of friction will cause the amplitude of a wave propagating onshore to go to zero at the coast. Equation (23) can be solved with $r \neq 0$ to obtain

$$\langle E_d \rangle = \mathcal{C}\frac{\exp\left(\frac{2r}{S\alpha^2}\frac{\sqrt{1-\frac{x^2}{x_c^2}}}{x}\right)}{x^2\sqrt{1-\frac{x^2}{x_c^2}}} \tag{25}$$

for a wave traveling onshore and

$$\langle E_d \rangle = \mathcal{C}\frac{\exp\left(-\frac{2r}{S\alpha^2}\frac{\sqrt{1-\frac{x^2}{x_c^2}}}{x}\right)}{x^2\sqrt{1-\frac{x^2}{x_c^2}}} \tag{26}$$

for a wave traveling offshore. These solutions contain only two length scales x_c and

$$K = 2rS^{-1}\alpha^{-2}, \tag{27}$$

so the solution is controlled by these two length scales. The length scale $K \equiv 2rS^{-1}\alpha^{-2}$ is not the frictional length scale. The frictional length scale, the distance defined by the group velocity times the friction timescale $2^{-1}r^{-1}D$, is

$$L_f = \frac{SD^2}{2r} = \frac{x^2}{K}. \tag{28}$$

The ratio of L_f to x_c, averaged inshore of x_c, is thus

$$\frac{L_f}{x_c} = \frac{x_c}{3K}. \tag{29}$$

When this ratio is large, the wave can travel over a distance of x_c without being dissipated. If the ratio is small, dissipation claims the wave before it can travel a distance comparable to x_c. Thus if $x_c \gg K$, the wave is little affected by friction, and if $x_c \ll K$, the wave is frictionally dominated. To illustrate this, the evolution of $\langle E_d \rangle^{1/2}$ has been computed for a wave that originates at -0.95x_c and travels to the coast. The square root of the energy density $\langle E_d \rangle^{1/2}$, which is proportional to the velocity amplitude of the wave, is plotted in Figure 3 for the inviscid, $x_c \gg K$, $x_c \approx K$, and $x_c \ll K$ cases. For the inviscid case, $\langle E_d \rangle^{1/2}$ goes to infinity as the wave approaches the coast. However, even with weak friction, $x_c \gg K$, $\langle E_d \rangle^{1/2}$ falls to zero as the wave approaches the coast. For both the $x_c \approx K$ and $x_c \ll K$ cases, $\langle E_d \rangle^{1/2}$ decreases monotonically toward the coast. Friction causes $\langle E_d \rangle$ to go to zero as the wave reaches the coast because the group velocity decreases linearly with the depth, and thus the wave takes infinitely long to reach the coast for any bottom topography whose slope remains finite and nonzero as the shore is approached. Since bottom friction has a finite timescale, the wave will be dissipated before it reaches the coast. Because of this, wave breaking or other nonlinear effects are not required to explain the disappearance of the internal waves as they propagate toward the coast, though they are not prohibited, either. Further, when $K \geq x_c$, $\langle E_d \rangle$ decays monotonically as the wave moves to the coast, and so internal waves are unlikely to break if $K \geq x_c$.

Figure 3

The severe dissipation of the internal waves before they reach the coast contrasts with the behavior of surface gravity waves and interfacial waves in a two-layer system. There is no fundamental difference between the

dynamics of these gravity waves, for the group velocities all scale with the square root of the top to bottom (or air/water) density difference and the square root of the water depth. However, the top to bottom (or air/water) density difference of the surface gravity waves and interfacial waves is constant across the shelf, while the top to bottom density difference in a continuously stratified fluid depends linearly on the water depth. Thus the group velocity of the surface gravity waves and the interfacial waves depends on the square root of the water depth, while the group velocity of the internal waves described here depends linearly on depth. Because of this, the surface gravity waves and interfacial waves reach the coast in a finite time while the internal gravity waves take an infinite time to reach the coast and thus are more dissipated by friction.

For a typical buoyancy frequency of 100 cpd and an r of 5×10^{-4} m s^{-1}, the frictional length scale K is of order 20 to 30 km for a mode 1 wave of 5-70 cycles per day over a typical United States west coast slope of 5×10^{-3}. For the same waves on a typical United States east coast slope of 1×10^{-3}, the length is 25 times longer, of order 500 to 750 km, and thus friction more completely attenuates waves during their passage over the broader east coast shelf. The frictional length scale increases as the frequency increases because, as seen in Figure 4, the group velocity and hence S decrease as frequency increases. However, this increase is order 1 until the frequency reaches $0.7N$.

Figure 4

From (24) and (26) it appears that the amplitude of a wave traveling offshore will go to infinity as it approaches $-x_c$. This is an artifact of the failure of ray tracing near the caustic at $-x_c$ [*Lighthill*, 1978]. The inviscid wave is reflected back from $-x_c$ with its amplitude unchanged. The outgoing frictional wave is also reflected back to the coast from $-x_c$, but only after loosing some energy to bottom friction in the caustic. This energy loss is quantified in the appendix. Once the wave is reflected back from the caustic, its energy density evolution is governed by (25).

5. Internal Waves in the Presence of a Barotropic Mean Flow

Horizontal mean currents can transfer energy to or from internal waves as the waves propagate across the shelf and can also cause caustics that reflect the waves back across the shelf. To analyze this effect, the alongshore flow is idealized as a barotropic current $V(x)$, which varies in the cross-shelf direction only. (*Olbers* [1981] studies an internal wave in an unbounded fluid with a vertically sheared mean flow and finds critical

layer phenomena not present in this barotropic work.) The effect of the mean currents on the strength of the bottom friction is not considered here, even though r, the strength of the linear bottom friction, depends on the strength of the mean currents in realistic models of bottom friction [*Wright and Thompson*, 1983].

The barotropic flow is assumed to be weakly sheared, so that the effective change in the local rate of rotation caused by the mean flow relative vorticity does not appreciably alter the dispersion relation for the intrinsic frequency of the wave, the frequency of the non-Doppler shifted wave given by (8). This is an assumption that the intrinsic frequency is several times f, so that a change in f does not affect the dispersion relation significantly, or an assumption that the mean flow has a low Rossby number. More formally, the effective Coriolis parameter of the flow found by *Kunze* [1985], $(f^2 + fV_x)^{1/2}$, can be substituted into the dispersion curve, (8), and the dispersion relation can be manipulated to find the criterion for neglecting V_x:

$$\frac{1}{2}\frac{\partial V}{\partial x} \ll \sqrt{f^2 + c^2 N^2}, \tag{30}$$

This criterion is easily met for realistic coastal flows and internal wave frequencies.

Within these assumptions the dispersion relation for modal internal waves can be written as

$$\omega = V(x) l_0 + \omega_r \left(k, l_0, M, D\right), \tag{31}$$

where ω_r is the intrinsic frequency found from the dispersion relation for the un-Doppler shifted wave (8). Since the mean flow does not vary in y or time, ω, l_0, and M are, as before, conserved along a ray. Because ω, l_0, and M do not vary, ω_r is constrained to remain between N, as $|k| \to \infty$, and $\omega_{\min}$, as $|k| \to 0$, where

$$\omega_{\min} = \omega_r \left(k = 0, l_0, M, D\right) = \sqrt{\frac{l_0^2 N^2 + f^2 \frac{M^2 \pi^2}{D^2}}{l_0^2 + \frac{M^2 \pi^2}{D^2}}}. \tag{32}$$

Thus the wave can only exist where

$$\omega_{\min} \leq \omega - V(x) l_0 \leq N. \tag{33}$$

The effects of a mean current on a ray will be small if the current does not alter the intrinsic frequency ω_r greatly. This is true when

$$\frac{V l_0}{\omega} \ll 1. \tag{34}$$

Solving for l_0 from the dispersion relation for un-Doppler shifted waves and assuming that $f^2 \ll \omega^2 \ll N^2$, this criterion is met if

$$V \ll \frac{N \alpha x_c}{M \pi}, \tag{35}$$

which, for N=100 cpd and $x_c = 30$ km, means $V \ll 30$ cm s^{-1}, and for an x_c of 60 km, $V \ll 60$ cm s^{-1}.

The energy E of the wave is not conserved in the presence of a mean sheared flow, for the mean flow can serve as an infinite source or sink of internal wave energy. However, *Lighthill* [1978] shows that the wave action

$$E_a = \frac{E}{\omega_r} \tag{36}$$

is conserved by a wave. Thus (16) becomes

$$\frac{\partial}{\partial x}\left(D\frac{\langle E_d\rangle}{\omega_r}\hat{i}\cdot\mathbf{c_{gr}}\langle E_d\rangle\right) = -\frac{T^{-1}D\langle E_d\rangle}{\omega_r}, \tag{37}$$

where the timescale of dissipation T is as before and $\mathbf{c_{gr}}$ is the group velocity of the un-Doppler shifted wave. $V(x)$ is absent from (37) because, by definition, no component of the mean flow is in the cross-shelf direction. It is not possible to get general solutions for arbitrary or realistic $V(x)$ profiles because of the complex dependence of $|\mathbf{c_{gr}}|$ on ω_r and thus $V(x)$. It is not difficult, however, to solve (37) with standard numerical techniques. More enlightening, however, is to examine some of the limits of (37).

If $f^2 \ll \omega_r^2 \ll N^2$, the wave is nondispersive, which allows $\mathbf{c_{gr}}$ to be approximated as

$$|\mathbf{c_{gr}}| = \frac{ND}{M\pi}. \tag{38}$$

Equation (37) can then be written as

$$\frac{\partial}{\partial x}\left(\frac{D^2N^2\alpha x_c l_0}{M^2\pi^2\omega_r^2}\right) = -\frac{T^{-1}D\langle E_d\rangle}{\omega_r}, \tag{39}$$

using (18) and the further assumption that $k^2+l_0^2 \gg l_0^2$, which, for the qualitative purposes of this discussion, is true when the wave is inshore of $-2/3x_c$. Because in these limits the cross-shelf group velocity is nearly constant and because wave dissipation by bottom friction depends on the cross-shelf group velocity, the amount the wave is dissipated as it crosses the shelf does not depend on the mean current in these limits. Thus the effect of the mean currents on the wave amplitude can be illustrated from the inviscid problem. From (39), but with $T = \infty$,

$$\langle E_d\rangle \propto \frac{\omega_r^2}{D^2}. \tag{40}$$

If V and l_0 have the same sign and the magnitude of V increases, ω_r is decreased and thus the amplitude of the wave decreases. If V and l_0 have differing signs

and the magnitude of V increases, ω_r is increased and the amplitude of the wave increases. Thus, like many other waves [*Lighthill*, 1978], an internal wave traveling over the shelf will take energy from a mean flow if its alongshore component of group velocity is against a strengthening mean flow and lose energy to the mean flow if the alongshore group velocity is with a strengthening mean flow.

Different phenomena arise when the condition $\omega_{\min}^2 \ll \omega_r^2 \ll N^2$ is not met. If Vl_0 increases to the point that $\omega_r \to \omega_{\min}$, then $k \to 0$, which produces a caustic of the same form as described earlier in the $x \to x_c$ case. As in the $x \to x_c$ caustic, the wave energy is reflected from whence it came. The infinite amplitude suggested by (37) as $|\mathbf{c_{gr}}|$ goes to zero does not occur, and instead, there is only a weak local maximum in $\langle E_d \rangle$ as in the $x \to x_c$ caustic. If the wave is between $-x_c$ and where $\omega_r \to \omega_{\min}$, it is trapped in a waveguide between these two caustics and propagates down the coast in the same direction as, but faster than, the mean flow.

If Vl_0 decreases to the point that $\omega_r \to N$, then $k \to \pm\infty$. Because $\omega_r \to N$, $|\mathbf{c_{gr}}| \to 0$, as illustrated in Figure 4. The ray-tracing theory does not break down, since as $k \to \pm\infty$, the horizontal scale of the wave becomes less. The ray does not get reflected back but, instead, asymptotically approaches the location where $\omega_r = N$. As in the case where the ray goes to the shore, friction dominates the cross-shelf evolution of $\langle E_d \rangle$ as $|\mathbf{c_{gr}}| \to 0$, causing the amplitude to go to zero. The local increase in $\langle E_d \rangle$and the subsequent decrease in $\langle E_d \rangle$ as friction begins to dominate are illustrated in Figure 5. This figure follows the square root of $\langle E_d \rangle$ along a ray launched near x_c, where $V = 0$, into a region where Vl_0 decreases. Because the wave entering the region where $\omega_r \to N$ is dissipated, there is no waveguide possible for internal waves traveling against the mean current; they must be dissipated either at the shore or where $\omega_r \to N$.

Figure 5

6. What a Current Meter Would Observe: No Mean Flow Case

The preceding sections have discussed the evolution of a single ray as it travels onshore or offshore. Since most observational techniques only measure currents or temperatures at a point, it is necessary to integrate over all the rays that go through a point to predict the currents at that point. This section illustrates how a very simple model of internal waves on the shelf can be used

to predict the observations at a current meter mooring. Vertical current resolution at a point is assumed to be dense enough to resolve the vertical modes. The observables discussed are the total power at a frequency and the ellipticity of the current ellipse at that frequency (The ellipticity is the square of the ratio of the major and minor axes of the current ellipse and is a useful measure of the anisotropy of the wave field).

The model assumes that, at the offshore boundary, there is an ensemble of waves of a given frequency propagating onshore that have the same amplitude, regardless of orientation. This assumption is unlikely to be valid in general, but, lacking better knowledge of the internal wave climate at the shelf break, it is a useful first assumption. This spectrum begins to feel the bottom at a distance offshore of x_b. As discussed above, x_b could be either where the line of $N = \omega$ intersects the bottom, where the bottom slope stops exceeding the characteristic slope of internal waves c, or where the bottom becomes flat. The mean alongshore current is taken to be zero in this section, but this assumption is relaxed in the next section. The bottom inshore of x_b has constant slope α as before.

The evolution of the energy density of a wave whose wave vector makes an angle of θ with the cross-shelf direction is, from (25),

$$\langle E_d \rangle = \frac{1}{\pi} \frac{x_b^2 \cos(\theta)}{x^2 \sqrt{1 - \frac{x^2}{x_b^2} \sin^2(\theta)}} \times \exp\left[\left(\frac{\sqrt{1 - \frac{x^2}{x_b^2} \sin^2(\theta)}}{x} - \frac{\cos(\theta)}{x_b} \right) \frac{2r}{S\alpha^2} \right]. \quad (41)$$

The wave energy density observed at a fixed site is the sum of the $\langle E_d \rangle$ of each wave moving past that site if the waves have random phase. The observed power at a single vertical mode and frequency, $\overline{\langle E_d \rangle}$, is thus the integral of (41) over $-90° \leq \theta \leq 90°$. This integral is simple to evaluate numerically.

To calculate ellipticity, however, it is necessary to calculate the power in the cross-shelf direction P_{uu} and the power in the alongshore direction P_{vv}. From the plane wave solution of the internal wave, (2),

$$P_{uu} = \langle E_d \rangle \left[\cos^2(\theta_m) + \frac{f^2}{\omega^2} \sin^2(\theta_m) \right], \quad (42a)$$

$$P_{vv} = \langle E_d \rangle \left[\sin^2(\theta_m) + \frac{f^2}{\omega^2} \cos^2(\theta_m) \right], \quad (42b)$$

where θ_m is the angle made by the wave vector with the cross-shelf direction at the current meter. From

(9), with depth $D = -\alpha x$;

$$\theta_m = \arctan \frac{l_0}{k} = \arctan \left[\frac{\sin(\theta)}{\sqrt{\frac{x_b^2}{x^2} - \sin^2(\theta)}} \right]. \quad (43)$$

The expressions for P_{uu} and P_{vv} must be integrated over all θ to account for all rays the current meters observe, which leads to an ellipticity of

$$\frac{\int_{-90^\circ}^{90^\circ} P_{uu} d\theta}{\int_{-90^\circ}^{90^\circ} P_{vv} d\theta}. \quad (44)$$

As with the power, the integrals are easily solved numerically.

The limits of ellipticity and power as x limits to x_b and the coast are visible by inspection. As x approaches x_b, $\langle E_d \rangle$ of a ray goes to π^{-1}, because that is the initial condition. The local angle θ_m will limit to θ at the same time. Thus the energy density observed by the current meter $\overline{\langle E_d \rangle}$, which is the integral of $\langle E_d \rangle$ over θ, will approach 1 as x goes to x_b. The ellipticity will also go to 1 as x goes to x_b. This recovers the initial condition of an isotropic wave field with an $\overline{\langle E_d \rangle}$ of 1.

It was shown in section 4 that even with infinitesimal bottom friction, $\langle E_d \rangle$ goes to 0 as x goes to 0, and thus the power integrated over all rays goes to 0 at the coast. The ellipticity, however, is the ratio of two powers and does not go to 0. As x goes to 0, θ_m approaches $\theta x/x_b$. Thus $\cos(\theta_m)$ limits to 1, $\sin(\theta_m)$ limits to $\theta x/x_b$, and (44) limits to ω^2/f^2. This is intuitively acceptable because as the waves approaches the shore, they becomes more tightly focused in the cross-shore direction, until all of the rays are headed almost directly inshore. The ellipticity then asymptotes to the single plane wave limit of ω^2/f^2.

The strength of friction does not affect the ellipticity significantly if the only internal wave signal on the shelf is that of the internal waves arriving from offshore. As seen in Figure 6, a factor of 16 increase in the ratio of K to x_b, from 0.25 to 4, greatly increases the attenuation of power going onshore but only marginally affects the ellipticity of the ensemble of waves. This is because the waves are very quickly turned toward the shore by the bathymetry, and the subsequent variation in the path length between waves of different orientation is minimal. The friction thus attenuates all waves to a similar extent.

Figure 6

Perhaps more surprisingly, the ellipticity is not strongly dependent on frequency or f until x/x_b becomes small, despite the fact that the ellipticity of a single plane wave, ω^2/f^2, depends strongly on the frequency and f. In Figure 7 the ellipticities of four en-

Figure 7

sembles of waves are plotted as a function of cross-shelf distance. Three of the ensembles consist of waves with a frequency of $10f$, $14f$, and $40f$, while the fourth ensemble of waves exists in an $f = 0$ ocean. The ellipticity of the ensemble of waves depends on f or ω only when the ellipticity of a single wave, ω^2/f^2, is comparable or less than the ellipticity of the $f = 0$ ensemble of waves. When this is not true, the ellipticity is dominated by the angular distribution of rays, not the ellipticity of the currents of each individual wave.

Friction does, however, play a strong role in the observed power. The higher the friction, the lower the power as one moves inshore. The plots of $\overline{\langle E_d \rangle}$ versus cross-shelf distance in Figure 6 have the same qualitative dependence on the ratio of K/x_b as the individual rays had to the ratio of K/x_c in previous sections. Since K increases with frequency and mode (see Figure 4), higher frequencies and higher modes are more attenuated as they move onshore. Thus, whatever the frequency spectrum at x_b, it should redden as one moves inshore and become more dominated by low-mode waves.

It is unrealistic to expect that the only internal waves on a shelf are the ones propagating from offshore. To represent the presence of waves generated on the shelf, the model has been modified to include an isotropic background noise whose amplitude is everywhere 10% of the energy density at x_b. This isotropic wave field is meant to be a representation of the waves generated on the shelf itself. It must be a poor model, if for no other reason than that the wave field generated on the shelf is unlikely to be isotropic. In the absence of some knowledge of the mechanism for the generation of internal waves on the shelf, it is unclear what would be more sensible, however. While the total internal wave energy is only slightly altered by the addition of the isotropic wave field, the observed ellipticity near the coast is dominated by the isotropic wave field, since the energy of the waves propagating from x_b has been attenuated by the passage across the shelf. This is clearly seen in Figure 8, in which the ellipticity and $\langle E_d \rangle$ are plotted for the same three ratios of K to x_b as in Figure 6, but with the added isotropic wave field. All of the ellipticities now approach 1 near the coast because the signal is dominated by the isotropic wave field near the coast, and the greater the friction, the faster the waves from offshore are attenuated and the more the isotropic wave field dominates the ellipticity. The lesson in this is not in the exact shape of the curves in Figure 8, since the model of waves generated on the shelf is naive, rather, the lesson is that the broader a

Figure 8

shelf is, or the stronger friction is, the less the propagation of waves from the deep ocean matters and the more the generation of waves on the shelf matters to the wave climate on the shelf. Because friction dissipates higher frequency and higher vertical modes more effectively, observations of higher frequency and higher mode waves will be more affected by the generation of waves on the shelf.

7. What a Current Meter Would Observe: Mean Flow Case

The model described in section 6 can be extended to include mean currents so that the anisotropy introduced by the mean currents can be studied. However, the interpretation of the results becomes more difficult. The problem lies not only in the prediction of the evolution of any given ray but also in the identification of which rays will have a frequency ω at the current meter and what the initial amplitude of those rays was. Because of this, an alongshelf current does not vary in the cross-shelf direction will have important effects that were not present in the analysis of single rays in the presence of mean flows. To make the extension of the model simpler, the shears are chosen to be small enough that ω_r does not go to $\omega_{\min}$, so no waves are reflected back to the shelf break. This assumption places constraints on the alongshore currents that can be surmised from (32).

The initial conditions of the rays at x_b are now modeled as a *Garrett and Munk* [1972] (hereafter referred to as GM) spectrum, even though the GM spectrum is not meant to be applicable near vertical or horizontal boundaries. Thus the amplitude of the internal waves at x_b is taken to depend on ω_r^{-2}. This means the spectrum is isotropic at x_b in the moving reference frame defined by $V(x_b)$ or, equivalently, the reference frame in which $V(x_b) = 0$ is special for the whole shelf. In any other reference frame the internal wave field at x_b is anisotropic, for waves at a given ω that are Doppler shifted from lower ω_r will have greater amplitudes than those Doppler shifted from higher ω_r. Thus waves traveling with the current (V and l_0 of the same sign) will be observed by a fixed observer at x_b to have greater amplitude then those moving against the current. Whether this is a correct initial condition depends on what sets the GM spectra and how quickly it equilibrates, questions that are not addressed here.

The solution for these initial conditions involves a straightforward substitution of (37) for (23) in the pre-

vious model with two modifications. The first is that a current meter observes not the energy density of a wave but, rather, the power in the horizontal currents. Thus (42) must be multiplied by the conversion from $\langle E_d \rangle$ to to horizontal current power given in (15) before (42) is integrated over all incoming rays. This conversion factor is a function of ω_r.

The second complication is that for a given angle θ of the horizontal wave vector to the onshore direction at x_b, there can be more than one ray with frequency ω. In order to find all the rays with a frequency ω and an angle θ, the dispersion relation (31) is written in terms of θ and the magnitude of the horizontal wave vector $|\mathbf{k}|$:

$$\pm\omega = |\mathbf{k}| \sin(\theta) + \sqrt{\frac{|\mathbf{k}|^2 N^2 + \frac{M^2\pi^2}{D^2} f^2}{|\mathbf{k}|^2 + \frac{M^2\pi^2}{D^2}}} \tag{45}$$

The plus/minus in front of ω is necessary to include all waves that a current meter would observe with a frequency ω. The intrinsic frequency ω_r must always be positive, as it is defined to be in (8), (31), and (45), so that the wave number vector $\mathbf{k}$ unambiguously indicates the direction of propagation of an un-Doppler shifted wave, but this does not constrain the sign of ω. The model first solves for $|\mathbf{k}|$ for an evenly spaced subset of all θ onshore, and then for each θ it traces the resulting rays toward the coast using (37). The total power and covariance are summed over all the possible waves. This is like the numerical integration over θ in section 6, but it includes the possibility of multiple rays at a given θ.

The anisotropy introduced by the addition of a mean current is quantified by examining the angle of the principal axis of the current ellipse to the cross-shore direction. This is derived from the energy density of each ray, again assuming that the waves have random phase. Following *Godin* [1988], the angle of the major axis is found from

$$\theta_{\mathrm{elip}_m} = \frac{1}{2} \arctan\left(\frac{2Co_{uv}}{P_{uu} - P_{vv}}\right), \tag{46}$$

where P_{uu} and P_{vv} are the cross-shore and alongshore powers as before, and Co_{uv} is the cospectrum of the alongshore and cross-shore velocities.

One source of anisotropy is the anisotropy in the initial amplitude of the rays at x_b caused by the dependence of ω_r on the orientation of the ray when $V(x_b) \neq 0$. This will tend to tilt θ_{elip_m} downstream, since waves moving with the current will have been Doppler shifted from a lower ω_r and thus have greater amplitude.

However, even when $V(x_b) = 0$ and the rays have the same amplitude when they leave x_b, the shear can alter the horizontal currents observed at a current meter. Not only can a mean sheared flow alter the energy density via the mechanisms outlined in section 5, but as ω_r increases, a given $\langle E_d \rangle$ produces less horizontal current power (equation (15)).

To describe the current meter observations in the presence of a mean shear flow, two mean current profiles will be examined. The first is a constant alongshore flow V_0. Since V is the same everywhere, ω_r is constant along a ray, and since ω_r is constant along a ray, only the effect of the anisotropy of the initial condition at x_b and the different K for each ray affect θ_{elip_m}. The other current profile varies from 0 at x_b linearly to V_0 at the shore. Since $\omega_r = \omega$ at x_b, all the rays start with the same amplitude and θ_{elip_m} is only affected by the change in ω_r along the ray.

The actual parameters used in the model runs are meant to resemble those for the CODE region on the northern Californian shelf. Data from this region are examined by *Pringle*, this issue. The bottom friction $r = 5 \times 10^{-4}$ m s^{-1}, the slope $\alpha = 5 \times 10^{-3}$, $x_b = 30$ km, $f = 1.24$ cpd, and $N = 100$ cpd. The magnitude of the current V_0 is chosen as 0.1 m s^{-1}, and each current profile is studied with ω equal to 10 and 40 cpd. These runs were repeated with different values of r, and the ellipticity and the orientation of the current ellipses were found to be insensitive to friction.

The first current profile, 10 cm s^{-1} everywhere, does not have a symmetric distribution of energy around $\theta_0 = 0$ because the intrinsic frequency ω_r and hence the initial power in each ray are asymmetric around $\theta = 0$. All rays oriented downstream ($\theta_0 > 0$) have $\omega_r < \omega$, and all upstream rays have $\omega_r > \omega$, giving the rays oriented downstream greater initial amplitudes. Because of this, the current ellipse formed by the ensemble of waves is oriented downstream. The angle of the major axis to the shore then limits to zero as the waves move toward the shore, as illustrated in Figure 9. This is because as the rays approach the shore, the angle they make to the cross-shelf direction goes to zero and thus the angle of the major axis of the current ellipse approaches zero.

Figure 9

There are no qualitative changes between the $\omega = 10$ and 40 cpd cases shown in Figure 9, though the power decays faster in the cross-shelf direction and the major axis angle θ_{elip_m} is greater in the 40 cpd case. The faster decay in power comes about because of the greater K for higher frequencies, and θ_{elip_m} is greater because the Doppler shifting around ω increases as l increases (see (31)).

When the model is run with an alongshore current varying linearly between $V(x_b) = 0$ and $V(0) = 10$ cm s^{-1}, shown in Figure 10, the angle of the major axis of the current ellipse is much less than it was when V was a constant 10 cm s^{-1}. This occurs because all the rays have the same initial amplitude at x_b when there is no current at x_b. This result remains true until (35) is not satisfied and the sheared mean currents generate a caustic that reflects some waves back offshore.

Figure 10

It is disturbing that the angle the major axis makes to the cross-shore direction is strongly affected by the mean currents at the shelf break, because this effect is caused by the assumption that the initial energy of the wave scales as ω_r^{-2}. This assumption is based only on the GM spectrum, which is not meant to hold near the shelf break. This dependence on the initial condition is also disturbing because the choice of x_b is arbitrary to the extent that it can be made greater, i.e. moved farther out into the ocean, with only minor modifications to the ray-tracing theory to account for a different bottom slope. Then the $V(x_b)$ that sets ω_r and thus the initial amplitude of the ray would be different, and thus what would propagate onto the shelf would be different. This is difficulty that can only be avoided by knowledge of what sets the *Garrett and Munk* [1972] spectrum in the deep ocean or what determines the internal wave climate at x_b.

8. Conclusions

The ray-tracing results for individual waves can be summarized in three points. (1) Unless the vertical mode assumption breaks down or ω becomes greater than N near the bottom, waves generated on the shelf cannot propagate into the deep ocean if the initial wave vector does not point nearly directly offshore. (2) In the absence of a horizontally sheared flow, all waves are dissipated as they approach the shore, and for reasonable values of friction, $x_c \leq K$, the amplitude of the wave need never increase as the wave propagates onshore, lessening the chance of wave breaking. (3) A horizontally sheared flow can reflect waves that are traveling in one direction alongshore, while the same flow can cause a wave traveling in the opposite alongshore direction to be dissipated. A wave whose alongshore component of group velocity is with the flow can be trapped between two isobaths by a sheared flow, while a wave moving against the mean flow would be dissipated by bottom friction in the current or against the coast.

The results of integrating over all internal waves passing through a location can be summarized in an additional four points. (1) The ellipticity of a current ellipse

at a given frequency is independent of the frequency for much of the shelf. (2) The greater friction or the wider the shelf, the more waves generated on the shelf will dominate the observations. (3) Higher-mode and higher-frequency waves are more dissipated by friction across the shelf, and so the frequency spectrum of waves propagating from the shelf break should become redder onshore. (4) A mean current at the shelf break will introduce an asymmetry in the internal wave field on the shelf, primarily because the modeled internal wave amplitude at the shelf break depends on the wave's intrinsic frequency at the shelf break.

This analysis provides only an incomplete understanding of the propagation of linear internal waves onto a shelf. The most important phenomena that are not considered in this analysis are baroclinic mean flows, time-varying mean flows, and mean flows that vary in the along-shelf direction. Baroclinic flows, as shown by *Olbers* [1981], can cause critical layers across which internal waves can cross vertically in only one direction. This would dramatically alter a vertical modal structure. Time-varying mean flows can change the frequency of an internal wave [*Lighthill*, 1978] and also lead to freely propagating waves generated by topographical irregularities [*Lamb*, 1994]. Alongshore variability in the mean flow would force alongshore variability in the internal waves. The waves could be focused or dispersed, leading to changes in the local internal wave power levels.

Even if the above mechanisms were perfectly understood, it would not be possible to understand the internal wave climate on the shelf without a better understanding of sources of internal waves on the shelf itself and the nature of the internal waves propagating from the deep sea and shelf break onto the shelf.

Appendix

In the derivations presented above it has been assumed that friction does not make an $O(1)$ change to the modal structure of the internal wave. Ray tracing and energy conservation were used to examine the gradual evolution of the internal wave solutions as the waves shoaled and dissipated. In order to confirm these approximate solutions and derive the energy lost in the offshore caustic, a bottom boundary condition is derived for a sloping bottom with bottom friction. The bottom boundary condition will be derived assuming that the boundary layer is "thin" in a sense described below. This bottom boundary condition will be used to define the sense in which friction is small and to diagnose the energy loss in the offshore caustic.

To derive the bottom boundary conditions, it is necessary to modify (1a) and (1b) so that the horizontal momentum equations have vertical stress divergence terms:

$$\frac{\partial u}{\partial t} - fv = -\frac{1}{\rho_0}\frac{\partial P}{\partial x} + \frac{\partial X}{\partial z} \qquad \text{(A1a)}$$

$$\frac{\partial v}{\partial t} + fu = -\frac{1}{\rho_0}\frac{\partial P}{\partial y} + \frac{\partial Y}{\partial z}. \qquad \text{(A1b)}$$

Following the derivations of *Clarke and Brink* [1985], but without making any geostrophic or semigeostrophic approximations, the volume conservation equation (1d) is integrated from the seafloor to the top of the boundary layer, which is defined as where the stress divergence becomes negligible. Thus

$$\int_{-D}^{-D+\delta} \nabla \cdot \mathbf{u}\, dz = w|_{-D}^{-D+\delta} + \int_{-D}^{-D+\delta} \frac{\partial u}{\partial x} dz + \int_{-D}^{-D+\delta} \frac{\partial v}{\partial y} dz = 0, \qquad \text{(A2)}$$

where δ is the boundary layer thickness. No flow through the bottom implies that $w = -u\partial D/\partial x$ at the bottom. Using this condition and the chain rule, (A2) becomes

$$w|_{-D+\delta} + \left[\frac{\partial}{\partial x}(D-\delta)\right] u|_{-D+\delta} + \int_{-D}^{-D+\delta} \frac{\partial u}{\partial x} dz + \int_{-D}^{-D+\delta} \frac{\partial v}{\partial y} dz = 0. \qquad \text{(A3)}$$

This equation states that the vertical velocity at the top of the boundary layer is equal to the velocity of water flowing into the boundary layer plus the convergence and divergence of the horizontal flow in the

bottom boundary layer. In order to evaluate this expression, it is necessary to assume that the horizontal derivatives of pressure do not vary significantly in the boundary layer, so that the integrals of pressure and its derivatives through the boundary layer are the pressure and its derivatives at the bottom of the boundary layer times the boundary layer thickness δ. This is consistent with a nearly modal solution if $\delta \ll DM^{-1}$. Eliminating the velocities from (A3) for the pressure and stress evaluated at $z = -D$, assuming that δ does not vary in x, and substituting $P(x,z)\exp[i(ly - \omega t)]$ for pressure (it is the only consistent form for a bathymetry that does not vary in y) leads to

$$\begin{aligned} & c^2\frac{\partial P}{\partial z} + \alpha\left(\frac{\partial P}{\partial x} + \frac{lf}{\omega}P\right) \\ & \quad - \left(\delta\frac{\partial^2 P}{\partial x^2} + \frac{\partial X}{\partial x} + \frac{lf}{\omega}\delta\frac{\partial P}{\partial x} - \frac{if}{\omega}\frac{\partial Y}{\partial x}\right) \\ & \quad - \left(-l^2\delta P + ilY - \frac{lf}{\omega}\delta\frac{\partial P}{\partial x} - \frac{lf}{\omega}X\right) = 0, \quad \text{(A4)} \end{aligned}$$

at $z = -D$ (α is the slope of the bottom). To evaluate the stress terms, a drag law must be chosen. As in the work of *Brink* [1988], the drag law is chosen to be linear so that $X = r\,u|_{-D}$ and $Y = r\,v|_{-D}$, where u and v are the inviscid velocities. Thus the stress is

$$X = \frac{-r}{\omega^2 - f^2}\left(i\omega\frac{\partial P}{\partial x} + iflP\right)\Big|_{z=-D} \quad \text{(A5a)}$$

$$Y = \frac{-r}{\omega^2 - f^2}\left(-\omega lP - f\frac{\partial P}{\partial x}\right)\Big|_{z=-D}. \quad \text{(A5b)}$$

The stress term in (A4) can be shown to be larger than the terms multiplied by δ if $1 \ll r\omega^{-1}\delta^{-1}$. This is not, in general, the case for internal waves, and thus this derivation retains the terms containing δ, unlike *Brink* [1988] and *Clarke and Brink* [1985]. The magnitude of δ will be discussed below. Equations (A4) and (A5) can be solved to give the bottom boundary condition

$$\begin{aligned} & c^2\frac{\partial P}{\partial z} + \alpha\left(\frac{\partial P}{\partial x} + \frac{lf}{\omega}P\right) \\ & \qquad + \frac{ir}{\omega}\left(1 + \frac{i\delta\omega}{r}\right)\left(\frac{\partial^2 P}{\partial x^2} - l^2 P\right) = 0 \quad \text{(A6)} \end{aligned}$$

at $z = -D$. With this boundary condition one can determine when friction is small in the sense that the inviscid vertical modal solution is changed only slightly. Vertical modes are useful, for they allow the field equation for the internal waves to be represented approximately as an ordinary differential equation, which makes the analysis in the body of the paper possible.

To examine friction, the bottom is assumed flat ($\alpha = 0$) and a field equation for pressure outside the bottom boundary layer is derived from (1a)-(1e)

$$\frac{\partial^2 P}{\partial x^2} - c^2 \frac{\partial^2 P}{\partial z^2} - l^2 P = 0. \tag{A7}$$

The top boundary condition is a rigid lid, which implies no vertical pressure gradient at the top. The inviscid solutions (r=δ=0) to (A7) for a flat bottom are

$$P = \cos\left(\frac{M\pi}{D} z\right) P(x) \qquad M = 1, 2, \ldots \infty. \tag{A8}$$

Assuming that the solution to the problem with friction can be found by perturbing M slightly [*Brink*, 1988], the solution

$$P = \cos\left[\frac{\pi}{D} M \left(1 + \epsilon_{\text{fric}}\right) z\right] P(x) \tag{A9}$$

is substituted into (A6), and, using (A7) to evaluate $\partial^2 P/\partial x^2 - l^2 P$, ϵ_{fric} is found to be

$$\epsilon_{\text{fric}} = \frac{ir}{\omega D}\left(1 + \frac{i\delta\omega}{r}\right), \quad |\epsilon| \ll 1. \tag{A10}$$

Here ϵ_{fric} is small, and hence the modal solution is approximately correct, if

$$\frac{r}{\omega D} \ll 1, \qquad \frac{\delta}{D} \ll 1, \tag{A11}$$

the latter condition already being necessary for the validity of (A6). Substituting the perturbed M into (A7) leads to (again, simplifying with the assumption $\epsilon_{\text{fric}} \ll 1$)

$$\frac{\partial^2 P}{\partial x^2} + \left[\frac{c^2\pi^2 M^2}{D^2}\left(1 + \frac{2ir}{\omega D} - \frac{2\delta}{D}\right) - l^2\right] P = 0. \tag{A12}$$

It can be seen from (A12) that, to first order in δD^{-1}, the magnitude of δ affects only the horizontal wavelength of the wave, not the rate of dissipation per unit length of the wave, and that the horizontal wavelength is altered to $O(\delta D^{-1})$ by δ. It can be shown by a similar scattering formalism that, when αc^{-1} is small,

$$\frac{\partial^2 P}{\partial x^2} + \left[\frac{c^2\pi^2 M^2}{D^2}\left(1 + \frac{2ir}{\omega D} - \frac{2\delta}{D}\right) - l^2\right] P + \frac{1}{x}\frac{\partial P}{\partial x} + O(\alpha^2 c^{-2}) = 0. \tag{A13}$$

So what is δ? It is, in general, less than the Ekman depth. For a constant eddy viscosity model,

$$\delta = \sqrt{\frac{A}{\omega}}, \tag{A14}$$

where A is an eddy viscosity that may depend on the mean current fields, surface waves, and many other disparate factors. For more sophisticated treatments of this issue, see *Sanford and Grant* [1987] and *Trowbridge and Madsen* [1984].

Ray tracing fails at the caustic where the ray approaches $-x_c$. Thus the ray-tracing theory developed in the main text cannot predict the amplitude of the wave leaving the caustic, given the amplitude of the wave entering the caustic. In the absence of friction, of course, the solution is easy; all waves are reversible, thus the outgoing wave has the same energy flux as the incoming wave but oriented away from the caustic. The calculation that follows predicts the amplitude of a ray leaving a caustic as a function of the amplitude and orientation of the incoming ray, the bathymetry, and the strength of friction.

The secular term in (A13) is neglected because it is reversable as a wave enters and then leaves the caustic. Equation (A13) can then be written as

$$k^2 = \frac{\zeta^2\left(1+\frac{2\epsilon_c x_c}{x}\right)}{x^2} - \frac{\zeta^2}{x_c^2} \tag{A15a}$$

$$\frac{\partial^2 P}{\partial x^2} + k^2 P = 0, \tag{A15b}$$

where

$$\zeta = \frac{M\pi c}{\alpha}, \tag{A16a}$$

$$\epsilon_c = \frac{ir}{\omega\alpha x_c}\left(1+\frac{i\delta\omega}{r}\right), \tag{A16b}$$

and x_c is as before. The ζ can be thought of as a scaled characteristic slope of an internal wave, and ϵ_c can be considered as the strength of friction at the caustic. Approximations in the main text require $\zeta \gg 1$ and $\epsilon_c \ll 1$. Following *Lighthill* [1978], k^2 can be expanded as a Taylor series around the caustic in the inviscid problem, where $x = -x_c$:

$$k^2 = (2+6\epsilon_c)\frac{\zeta^2}{x_c^3}(x+x_c) + \frac{\zeta^2\epsilon_c}{x_c^2}. \tag{A17}$$

This implies a solution to P of

$$P = Ai\left\{-\left((2+6\epsilon_c)\frac{\zeta^2}{x_c^3}\right)^{\frac{1}{3}}\left[x + x_c\left(1+\epsilon_c\right)\right]\right\}, \tag{A18}$$

where Ai is the Airy function. This is a good approximation of the solution to P as long as the Taylor expansion of k^2 is valid, which it is when

$$\frac{2}{3}x_c \gg x + x_c. \tag{A19}$$

Equation (A18) can be analyzed with WKBJ/ray-tracing methods when

$$x + x_c > 2^{-\frac{1}{3}} \zeta^{-\frac{2}{3}} x_c \tag{A20}$$

[*Lighthill*, 1978]. Where (A18) (and thus (A15)) can be ray traced, the ray solutions derived in the main text can be equated to the rays leaving and entering the caustic, and thus the amplitude of a wave leaving the caustic can be found from the amplitude of a wave entering a caustic. It is best to fit the rays to the Airy function approximation inside the region where the WKBJ approximation to (A18) is valid or, from (A20), when

$$x_{\text{good}} = \beta 2^{-\frac{1}{3}} \zeta^{-\frac{2}{3}} x_c - x_c, \tag{A21}$$

where β is an $O(1)$ positive constant. The choice of β is somewhat arbitrary, but as it gets larger, the WKBJ approximation to the Airy function becomes more accurate but the Airy function approximation to (A15) becomes less accurate. Both the Airy function approximation to (A15) and the WKBJ approximation to the Airy function are valid at x_{good} when both (A20) and (A19) are true or when

$$\frac{2^{\frac{4}{3}}}{3\beta} \gg \zeta^{-\frac{2}{3}}. \tag{A22}$$

The WKBJ/ray-tracing approximation to (A18) is

$$\begin{aligned} &P_{\text{airyWKBJ}} = \\ &\quad \frac{1}{\sqrt{\pi}} \left[\left(1 + 6\epsilon_c\right) \zeta^2 x_c^{-3} \right]^{-\frac{1}{12}} \left[x + x_c \left(1 + \epsilon_c\right) \right]^{-\frac{1}{4}} \\ &\quad \times \cos \left\{ \frac{2}{3} \left(1 + 6\epsilon_c\right)^{\frac{1}{2}} \zeta x_c^{-\frac{3}{2}} \left[x + x_c \left(1 + \epsilon_c\right) \right]^{\frac{3}{2}} - \frac{\pi}{4} \right\} \end{aligned} \tag{A23}$$

[*Lighthill*, 1978]. The ray-tracing approximation to the incoming and outgoing waves is locally

$$P_{\text{rays}} = P_{\text{in}} e^{-ikx} + P_{\text{out}} e^{ikx}, \tag{A24}$$

where P_{in} is the amplitude of the wave entering the caustic, P_{out} is the amplitude of the wave leaving the caustic, and k is the x wave number from (A15a). Equation (A24) can be solved for the amplitude of P_{in} and P_{out} as a function of P_{rays} and its derivative in x, and then P_{airyWKBJ} can be substituted for P_{rays}, giving

$$\begin{aligned} &|P_{\text{in}}| = \\ &\qquad 0.5 \left| P_{\text{airyWKBJ}} + ik^{-1} \frac{\partial P_{\text{airyWKBJ}}}{\partial x} \right| \end{aligned} \tag{A25a}$$

$$|P_{\text{out}}| = 0.5 \left| P_{\text{airyWKBJ}} - ik^{-1} \frac{\partial P_{\text{airyWKBJ}}}{\partial x} \right| \quad \text{(A25b)}$$

Evaluating the ratio of P_{out} to P_{in} at x_{good} gives the amplitude lost in the caustic and between the caustic and x_{good}. It is sensitive to β only insofar as some energy is lost between the caustic and x_{good}. A β of 1.5 is found to work well in numerical solutions of (A15a) and (A15b).

The expression gained from substituting (A21), (A18), and (A15a) into (A25a) is unwieldy, but the amplitude loss, the ratio of $|P_{\text{out}}|$ to $|P_{\text{in}}|$, can be easily contoured. Because ϵ_c contains α and ω in a different combination, $(\omega\alpha)$, than does ζ [approximately $(\omega\alpha^{-1})$], it makes no sense to hold ϵ_c constant as ζ is varied. Thus for Figure A1 the amplitude loss is plotted with ϵ_c varying as it would when ζ varies because ω varies and α is constant, and in Figure A2, ϵ_c varies as it would when ζ varies because α varies and ω is constant.

Figure A1

Figure A2

Acknowledgments. This paper originated in Jay Austin's remark that internal waves should refract toward shore as surface gravity waves do. It was nurtured by many interesting talks with Lyn Harris, William Williams, Jay Austin, and Sarah Gille. It was greatly improved by the close readings given it by Steven Lentz. Two anonymous reviewers gave helpful comments. The work was funded by an Office of Naval Research fellowship and Office of Naval Research AASERT fellowship, N00014-95-1-0746. Further support was provided through Office of Naval Research grant N00014-92-J-1528. Woods Hole Oceanographic Institution contribution 9600.

References

Brink, K. H., On the effect of bottom friction on internal waves, *Cont. Shelf Res.*, *8(*4), 397–403, 1988.

Chapman, D. C., and M. C. Hendershott, Scattering of internal waves obliquely incident upon a step change in bottom relief, *Deep Sea Res., Part A, 28A(*11), 1323–1338, 1981.

Clarke, A. J., and K. H. Brink, The response of stratified, frictional flow of shelf and slope waters to fluctuating large-scale low-frequency wind forcing, *J. Phys. Oceanogr.*, *15*, 439–453, 1985.

Garrett, C., and W. Munk, Space-time scales of internal waves, *Geophys. Fluid Dyn.*, *3*, 225–264, 1972.

Godin, G., *Tides*, Cent. de Invest. Cient. y de Educ. Super. de Ensenada, Ensenada, Baja California, Mexico, 1988.

Kunze, E., Near-inertial wave propagation in geostrophic shear, *J. Phys. Oceanogr.*, *15*, 544–565, 1985.

Lamb, K. G., Numerical experiments of internal wave generation by strong tidal flow across a finite amplitude bank edge, *J. Geophys. Res.*, *99(C*1), 843–864, 1994.

LeBlond, P. H., and L. A. Mysak, *Waves in the Ocean*, Elsevier Sci., New York, 1978.

Lighthill, J., *Waves in Fluids*, Cambridge Univ. Press, New York, 1978.

McKee, W. D., Internal-inertial waves in a fluid of variable depth, *Proc. Cambridge Philos. Soc.*, *73*, 205–213, 1973.

Olbers, D. J., The propogation of internal waves in a geostrophic current, *J. Phys. Oceanogr.*, *11*, 1224–1233, 1981.

Pringle, J. M., Observations of high frequency internal waves in the Coastal Ocean Dynamics Experiment region, *J. Geophys. Res.*, this issue.

Sanford, L. P., and W. D. Grant, Dissipation of internal wave energy in the bottom noundary layer on the continental shelf, *J. Geophys. Res.*, *92(C*2), 1828–1844, 1987.

Trowbridge, J., and O. S. Madsen, Turbulent wave boundary layers, 1, Model formulation and first-order solution , *J. Geophys. Res.*, *89(C*5), 7989–7997, 1984.

Wright, D. G., and K. R. Thompson, Time-averaged forms of the nonlinear stress law, *J. Phys. Oceanogr.*, *13*, 341–345, 1983.

Wunsch, C., Progressive internal waves on slopes, *J. Fluid Mech.*, *35*, 131–144, 1969.

James Pringle, Scripps Institution of Oceanography, Univerisity of California, San Diego, Mail Stop 0218, La Jolla, CA 92093-0218 (email: pringle@alum.mit.edu)

Kenneth H. Brink, Mail Stop 28, Woods Hole Oceanographic Institution, Woods Hole, MA, 02543.

(Received July 18, 1997; revised July 29, 1998;
accepted September 21, 1998.)

[1]Now at Scripps Institution of Oceanography, University of California, San Diego, La Jolla.

Paper number 1998JC900054.
0148-0227/98/1998JC900054$09.00

Figure 1. (left) Mode 1 horizontal velocity structure for the stratification in Figure 2 is plotted for two differing frequencies, 2 and 40 cpd. (right) Same velocity structure plotted for two differing stratifications, the buoyancy frequency N constant and N from Figure 2.

Figure 1. (left) Mode 1 horizontal velocity structure for the stratification in Figure 2 is plotted for two differing frequencies, 2 and 40 cpd. (right) Same velocity structure plotted for two differing stratifications, the buoyancy frequency N constant and N from Figure 2.

Figure 2. Average buoyancy profile for July 1982 at 130 m depth in the Coastal Ocean Dynamics Region (CODE) region of coastal California [*Pringle*, this issue].

Figure 2. Average buoyancy profile for July 1982 at 130 m depth in the Coastal Ocean Dynamics Region (CODE) region of coastal California [*Pringle*, this issue].

Figure 3. Evolution of the square root of the energy density $\langle E_d \rangle$ as a function of offshore distance for the internal wave traveling from $-0.95x_c$ to the coast. An inviscid wave, a nearly inviscid $x_c \gg K$ wave, an intermediate friction $x_c \approx K$ wave, and a frictionally dominated $x_c \ll K$ wave are plotted.

Figure 3. Evolution of the square root of the energy density $\langle E_d \rangle$ as a function of offshore distance for the internal wave traveling from $-0.95x_c$ to the coast. An inviscid wave, a nearly inviscid $x_c \gg K$ wave, an intermediate friction $x_c \approx K$ wave, and a frictionally dominated $x_c \ll K$ wave are plotted.

Figure 4. (top) S as defined by (19a) and (19b). When multiplied by depth, S gives the group velocity of the wave for a mode 1 wave with N=100 cpd and inertial frequency f=1.24 cpd. A mode 2 wave would have half the speed, a mode three wave one third the speed, etc. (bottom) Frictional length scale K as a function of frequency. It is for a bottom drag of r=5×10^{-4} m s^{-1} and a bottom slope of 5×10^{-3}. All other parameters are as in Figure 4 (top). If the wave were mode 2, the length scale would be twice as large because the group speed would be half as large.

Figure 4. (top) S as defined by (19a) and (19b). When multiplied by depth, S gives the group velocity of the wave for a mode 1 wave with N=100 cpd and inertial frequency f=1.24 cpd. A mode 2 wave would have half the speed, a mode three wave one third the speed, etc. (bottom) Frictional length scale K as a function of frequency. It is for a bottom drag of r=5×10^{-4} m s^{-1} and a bottom slope of 5×10^{-3}. All other parameters are as in Figure 4 (top). If the wave were mode 2, the length scale would be twice as large because the group speed would be half as large.

Figure 5. Square root of $\langle E_d \rangle$ for a wave launched from 60 km offshore into a region where the mean currents are becoming more negative. The point where $\omega_r = N$ is 10 km offshore. N=100 cpd, f=1.24 cpd, and ω is 20 cpd. The current goes linearly from 0 at 60 km offshore to -2.8 m s^{-1} at 10 km offshore.

Figure 5. Square root of $\langle E_d \rangle$ for a wave launched from 60 km offshore into a region where the mean currents are becoming more negative. The point where $\omega_r = N$ is 10 km offshore. N=100 cpd, f=1.24 cpd, and ω is 20 cpd. The current goes linearly from 0 at 60 km offshore to -2.8 m s^{-1} at 10 km offshore.

Figure 6. (top) Ellipticity observed by current meters at a frequency of $10f$ for three different values of Kx_b^{-1}, 0.25 for weak friction, 1 for intermediate friction, and 4 for strong friction. (bottom) Energy density observed by a current meter for the same three ratios of K/x_b. The cross-shore distance has been normalized by x_b.

Figure 6. (top) Ellipticity observed by current meters at a frequency of $10f$ for three different values of Kx_b^{-1}, 0.25 for weak friction, 1 for intermediate friction, and 4 for strong friction. (bottom) Energy density observed by a current meter for the same three ratios of K/x_b. The cross-shore distance has been normalized by x_b.

Figure 7. Ellipticity of the current ellipse observed at frequencies of 10, 14, and 40 times f, as well as the ellipticity observed in an f=0 ocean, as a function of the cross-shore distance normalized by x_b. $K = x_b$.

Figure 7. Ellipticity of the current ellipse observed at frequencies of 10, 14, and 40 times f, as well as the ellipticity observed in an f=0 ocean, as a function of the cross-shore distance normalized by x_b. $K = x_b$.

Figure 8. Same as Figure 6, except with an isotropic noise field added whose $\overline{\langle E_d \rangle}$ is 10% of the $\overline{\langle E_d \rangle}$ at x_b. Notice that the ellipticities are so greatly reduced by the addition of the noise that the scale in the top panel is different from Figure 6.

Figure 8. Same as Figure 6, except with an isotropic noise field added whose $\overline{\langle E_d \rangle}$ is 10% of the $\overline{\langle E_d \rangle}$ at x_b. Notice that the ellipticities are so greatly reduced by the addition of the noise that the scale in the top panel is different from Figure 6.

Figure 9. Current meter observation model for the depth-averaged barotropic velocity V=10 cm s^{-1} case. (left) Evolution of the horizontal current power observed by a current meter as a function of cross-shelf distance and (right) angle that the major axis of the current ellipse makes with the cross-shelf direction.

Figure 9. Current meter observation model for the depth-averaged barotropic velocity V=10 cm s^{-1} case. (left) Evolution of the horizontal current power observed by a current meter as a function of cross-shelf distance and (right) angle that the major axis of the current ellipse makes with the cross-shelf direction.

Figure 10. Same as Figure 9, but for the case where V varies linearly between 10 cm s^{-1} at x_b and 0 at the coast and with the scale of θ_{elip_m} (right) reduced.

Figure 10. Same as Figure 9, but for the case where V varies linearly between 10 cm s^{-1} at x_b and 0 at the coast and with the scale of θ_{elip_m} (right) reduced.

Figure A1. Amplitude lost in a caustic as given by $\left|P_{\rm out}P_{\rm in}^{-1}\right|$, with ϵ_c calculated as a function of ζ and x_c, assuming that α and r are constant and ω varies. The ω for a mode 1 wave is given at the right. Since $\zeta \propto M^{-1}$, a mode 2 wave has a ζ that is half that of a mode 1 wave. The thick, nearly vertical line delimits where the solution is invalid because ϵ_c is no longer small, and the thick horizontal line delimits where (A22) fails.

Figure A1. Amplitude lost in a caustic as given by $\left|P_{\rm out}P_{\rm in}^{-1}\right|$, with ϵ_c calculated as a function of ζ and x_c, assuming that α and r are constant and ω varies. The ω for a mode 1 wave is given at the right. Since $\zeta \propto M^{-1}$, a mode 2 wave has a ζ that is half that of a mode 1 wave. The thick, nearly vertical line delimits where the solution is invalid because ϵ_c is no longer small, and the thick horizontal line delimits where (A22) fails.

Figure A2. Amplitude lost in a caustic as given by $\left|P_{\rm out}P_{\rm in}^{-1}\right|$ with ϵ_c calculated as a function of ζ and x_c, assuming that ω and r are constant and α varies. The α for a mode 1 wave is given at the right. Since $\zeta \propto M^{-1}$, a mode 2 wave has a ζ that is half that of a mode 1 wave. The thick line delimits where the solution is invalid because ϵ_c is no longer small.

Figure A2. Amplitude lost in a caustic as given by $\left|P_{\rm out}P_{\rm in}^{-1}\right|$ with ϵ_c calculated as a function of ζ and x_c, assuming that ω and r are constant and α varies. The α for a mode 1 wave is given at the right. Since $\zeta \propto M^{-1}$, a mode 2 wave has a ζ that is half that of a mode 1 wave. The thick line delimits where the solution is invalid because ϵ_c is no longer small.

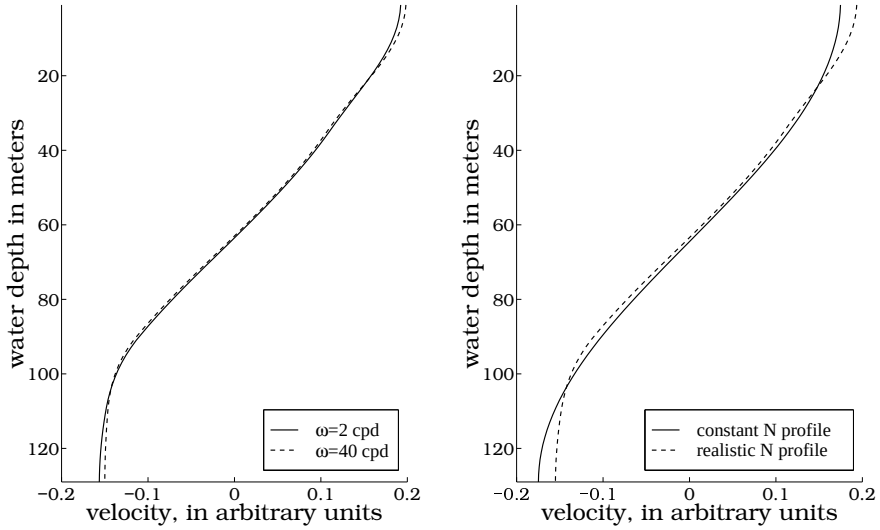
water depth in meters
20
40
60
80
100
120
−0.2
−0.1
0
0.1
0.2
velocity, in arbitrary units
ω=2 cpd
ω=40 cpd
water depth in meters
20
40
60
80
100
120
−0.2
−0.1
0
0.1
0.2
velocity, in arbitrary units
constant N profile
realistic N profile

Figure 1

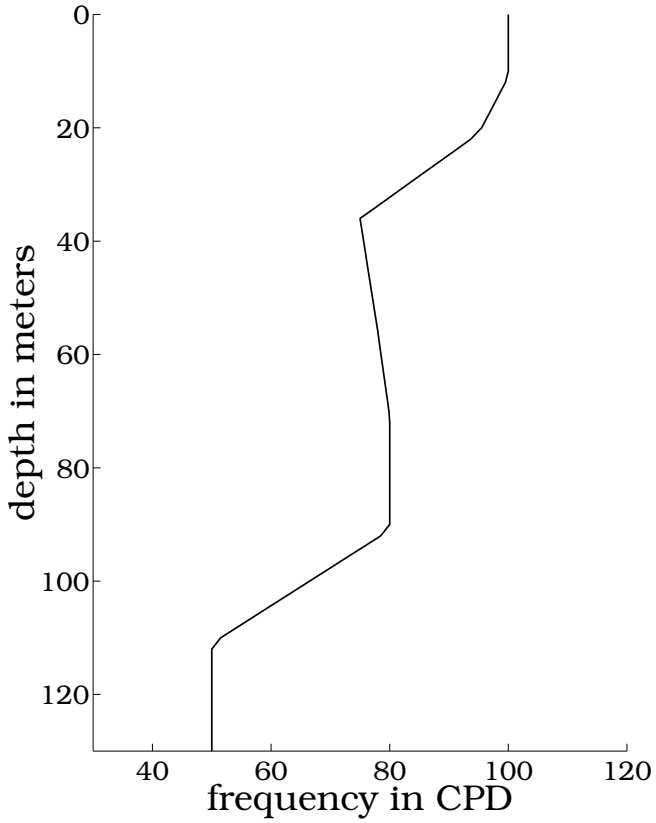
0
20
40
60
80
100
120
depth in meters
40
60
80
100
120
frequency in CPD

Figure 2

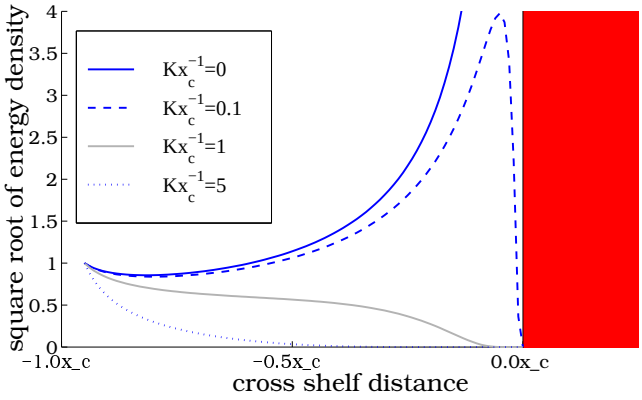
square root of energy density
cross shelf distance
−1.0x_c
−0.5x_c
0.0x_c
Kx_c^−1=0
Kx_c^−1=0.1
Kx_c^−1=1
Kx_c^−1=5

Figure 3

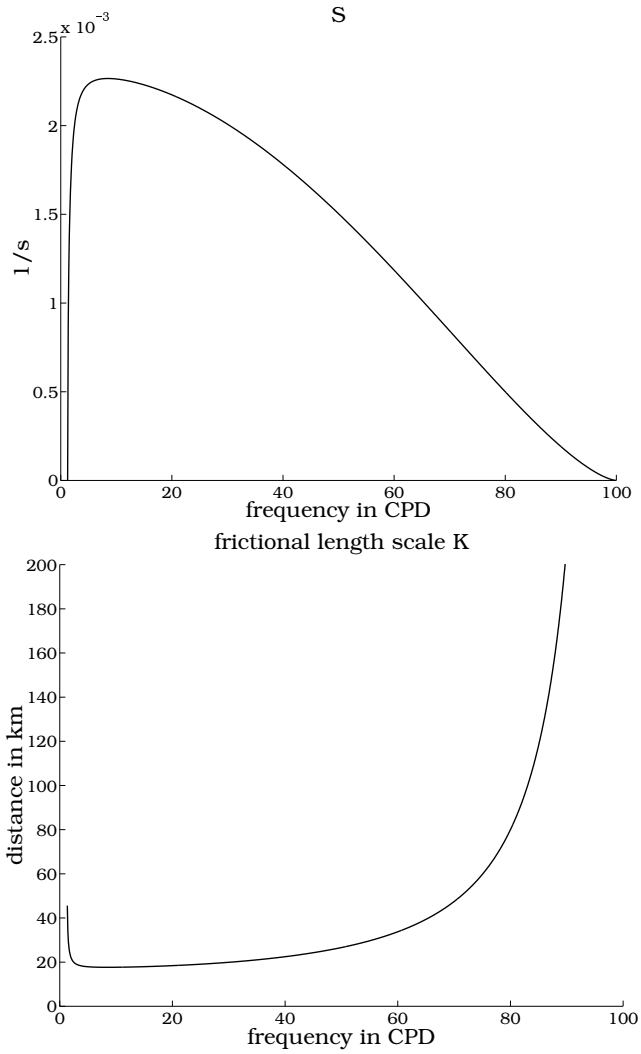
S
x 10^-3
2.5
2
1.5
1
0.5
0
1/s
0
20
40
60
80
100
frequency in CPD
frictional length scale K
200
180
160
140
120
100
80
60
40
20
0
distance in km
0
20
40
60
80
100
frequency in CPD

Figure 4

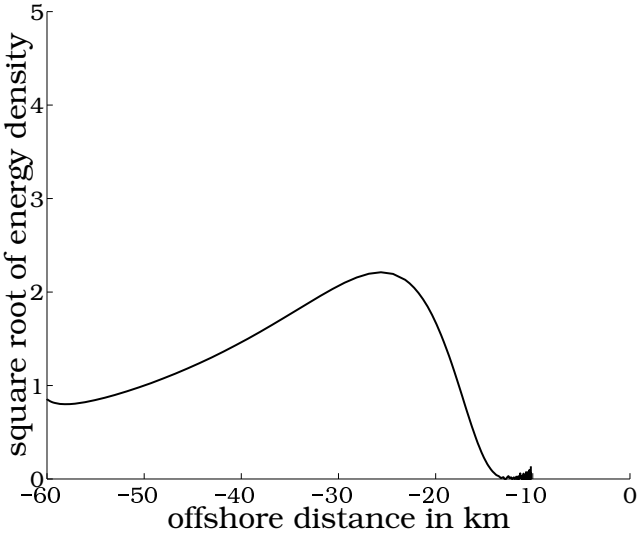
square root of energy density
offshore distance in km
0
1
2
3
4
5
−60
−50
−40
−30
−20
−10
0

Figure 5

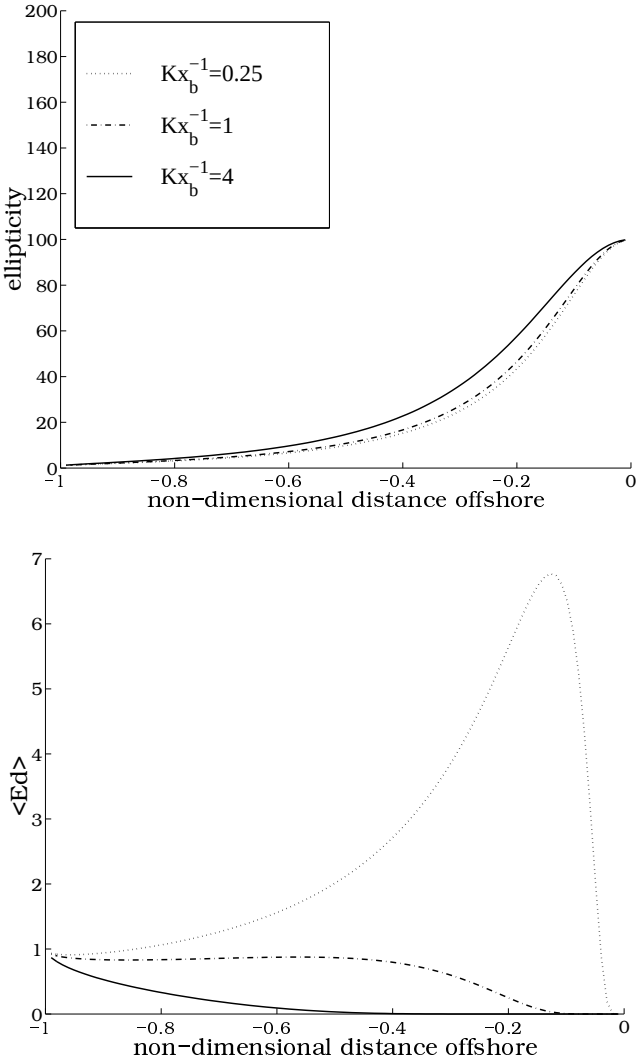
ellipticity
non−dimensional distance offshore
Kx_b^{-1}=0.25
Kx_b^{-1}=1
Kx_b^{-1}=4
<Ed>
non−dimensional distance offshore

Figure 6

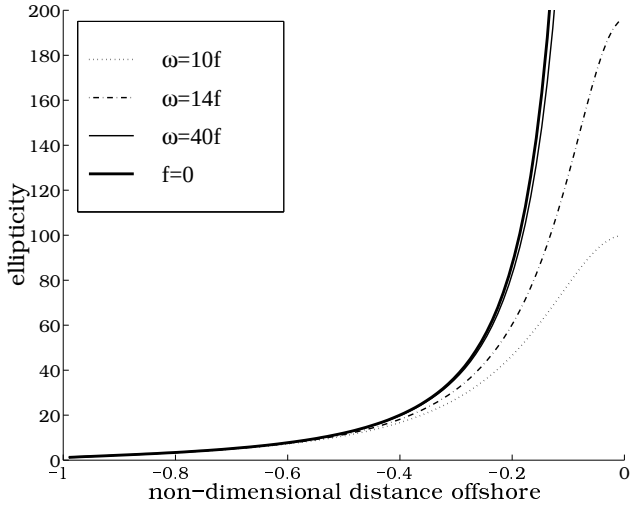
ω=10f
ω=14f
ω=40f
f=0
ellipticity
non−dimensional distance offshore
200
180
160
140
120
100
80
60
40
20
0
−1
−0.8
−0.6
−0.4
−0.2
0

Figure 7

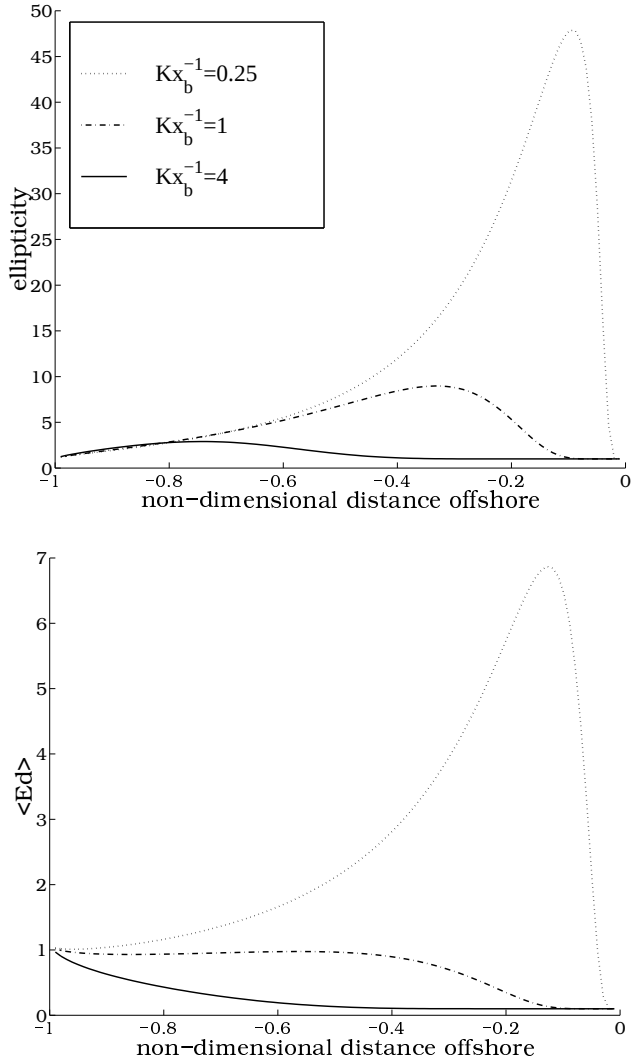
ellipticity
non−dimensional distance offshore
Kx_b^−1=0.25
Kx_b^−1=1
Kx_b^−1=4
<Ed>
non−dimensional distance offshore

Figure 8

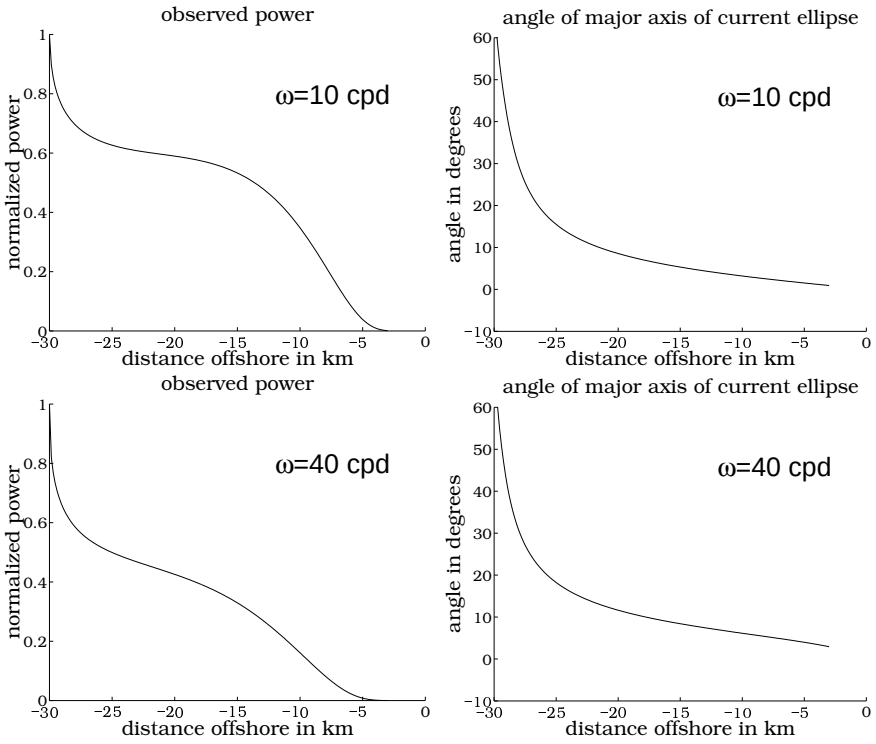
observed power
ω=10 cpd
normalized power
distance offshore in km
angle of major axis of current ellipse
ω=10 cpd
angle in degrees
distance offshore in km
observed power
ω=40 cpd
normalized power
distance offshore in km
angle of major axis of current ellipse
ω=40 cpd
angle in degrees
distance offshore in km

Figure 9

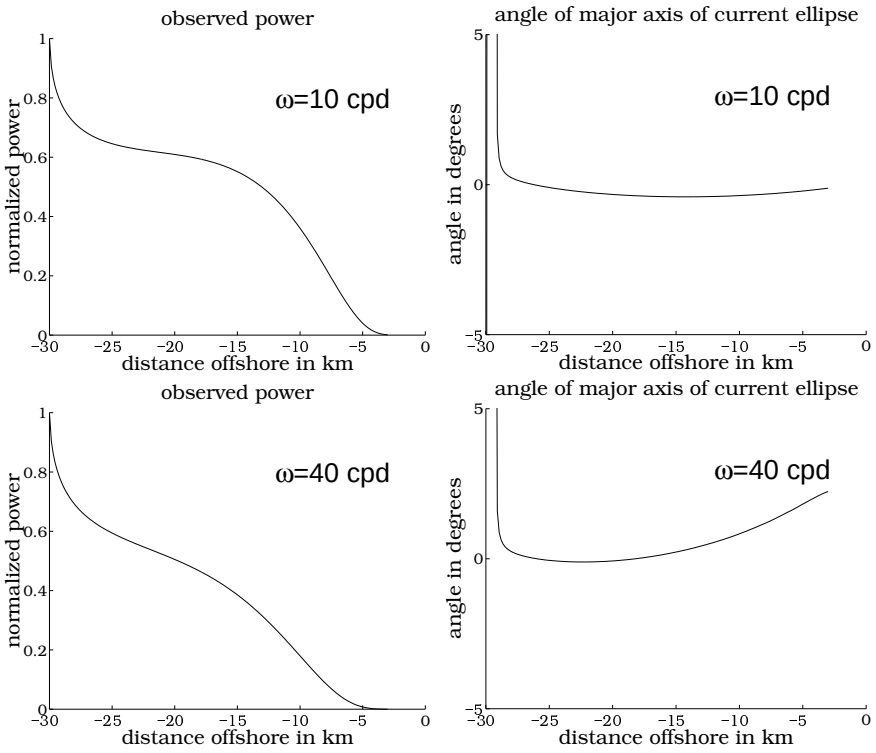
observed power
ω=10 cpd
normalized power
distance offshore in km
angle of major axis of current ellipse
ω=10 cpd
angle in degrees
distance offshore in km
observed power
ω=40 cpd
normalized power
distance offshore in km
angle of major axis of current ellipse
ω=40 cpd
angle in degrees
distance offshore in km

Figure 10

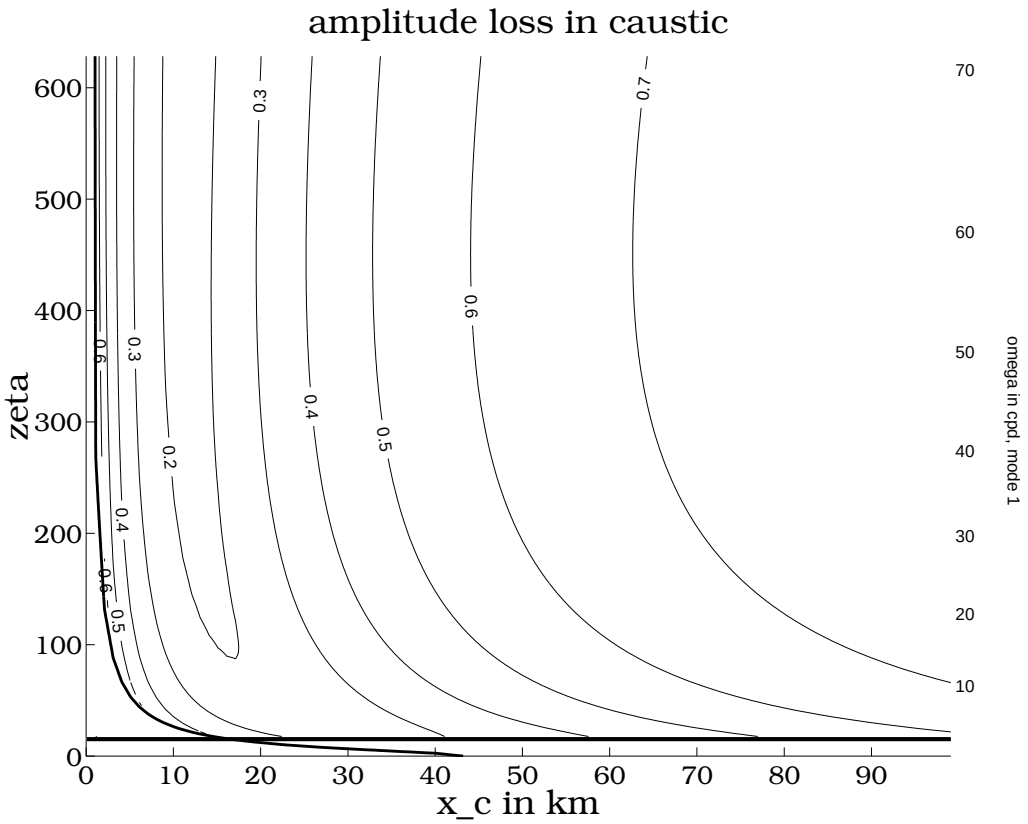
amplitude loss in caustic
zeta
x_c in km
omega in cpd, mode 1
0
100
200
300
400
500
600
0
10
20
30
40
50
60
70
80
90
10
20
30
40
50
60
70
0.1
0.2
0.3
0.4
0.5
0.6
0.7
0.8
0.9

Figure A1

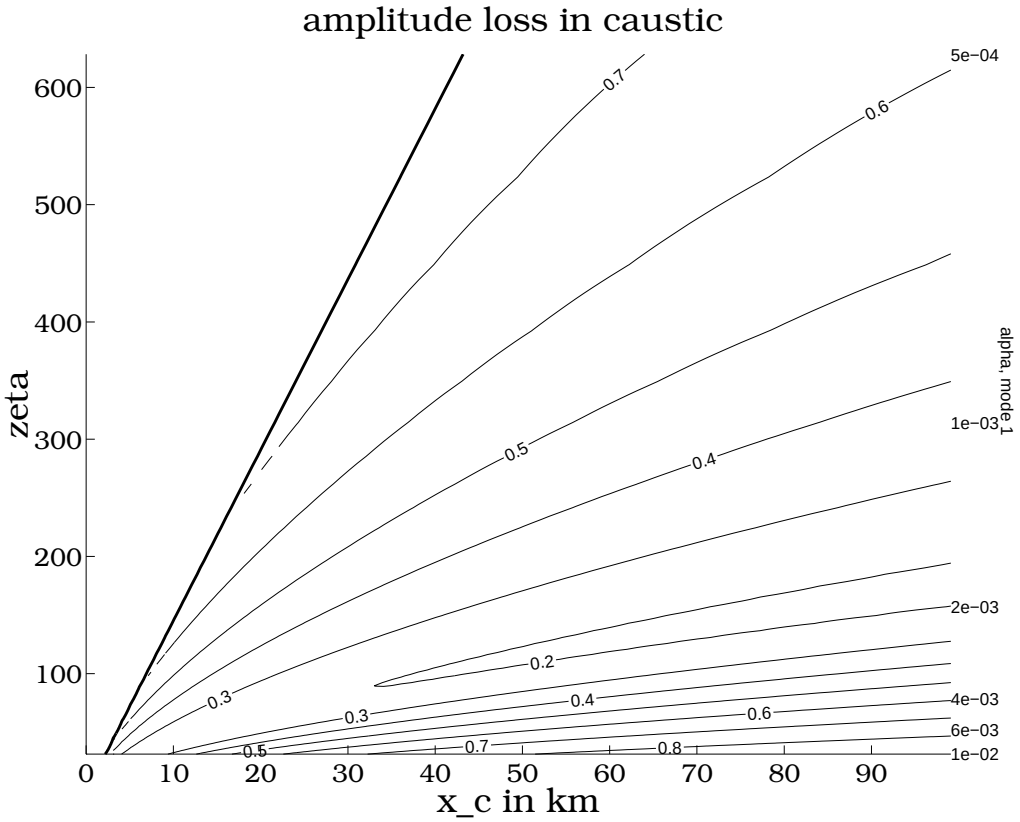
amplitude loss in caustic
zeta
x_c in km
alpha, mode1
5e−04
1e−03
2e−03
4e−03
6e−03
1e−02
0.7
0.6
0.5
0.4
0.3
0.2
0.3
0.4
0.6
0.5
0.7
0.8
600
500
400
300
200
100
0
10
20
30
40
50
60
70
80
90

Figure A2

PRINGLE AND BRINK: HIGH-FREQUENCY INTERNAL WAVES ON A SLOPING SHELF

PRINGLE AND BRINK: HIGH-FREQUENCY INTERNAL WAVES ON A SLOPING SHELF

PRINGLE AND BRINK: HIGH-FREQUENCY INTERNAL WAVES ON A SLOPING SHELF

PRINGLE AND BRINK: HIGH-FREQUENCY INTERNAL WAVES ON A SLOPING SHELF

PRINGLE AND BRINK: HIGH-FREQUENCY INTERNAL WAVES ON A SLOPING SHELF

PRINGLE AND BRINK: HIGH-FREQUENCY INTERNAL WAVES ON A SLOPING SHELF

PRINGLE AND BRINK: HIGH-FREQUENCY INTERNAL WAVES ON A SLOPING SHELF

PRINGLE AND BRINK: HIGH-FREQUENCY INTERNAL WAVES ON A SLOPING SHELF

PRINGLE AND BRINK: HIGH-FREQUENCY INTERNAL WAVES ON A SLOPING SHELF

PRINGLE AND BRINK: HIGH-FREQUENCY INTERNAL WAVES ON A SLOPING SHELF

PRINGLE AND BRINK: HIGH-FREQUENCY INTERNAL WAVES ON A SLOPING SHELF

PRINGLE AND BRINK: HIGH-FREQUENCY INTERNAL WAVES ON A SLOPING SHELF

PRINGLE AND BRINK: HIGH-FREQUENCY INTERNAL WAVES ON A SLOPING SHELF

PRINGLE AND BRINK: HIGH-FREQUENCY INTERNAL WAVES ON A SLOPING SHELF

PRINGLE AND BRINK: HIGH-FREQUENCY INTERNAL WAVES ON A SLOPING SHELF

PRINGLE AND BRINK: HIGH-FREQUENCY INTERNAL WAVES ON A SLOPING SHELF

PRINGLE AND BRINK: HIGH-FREQUENCY INTERNAL WAVES ON A SLOPING SHELF

PRINGLE AND BRINK: HIGH-FREQUENCY INTERNAL WAVES ON A SLOPING SHELF

PRINGLE AND BRINK: HIGH-FREQUENCY INTERNAL WAVES ON A SLOPING SHELF

PRINGLE AND BRINK: HIGH-FREQUENCY INTERNAL WAVES ON A SLOPING SHELF

PRINGLE AND BRINK: HIGH-FREQUENCY INTERNAL WAVES ON A SLOPING SHELF

PRINGLE AND BRINK: HIGH-FREQUENCY INTERNAL WAVES ON A SLOPING SHELF

PRINGLE AND BRINK: HIGH-FREQUENCY INTERNAL WAVES ON A SLOPING SHELF

PRINGLE AND BRINK: HIGH-FREQUENCY INTERNAL WAVES ON A SLOPING SHELF

PRINGLE AND BRINK: HIGH-FREQUENCY INTERNAL WAVES ON A SLOPING SHELF

PRINGLE AND BRINK: HIGH-FREQUENCY INTERNAL WAVES ON A SLOPING SHELF

PRINGLE AND BRINK: HIGH-FREQUENCY INTERNAL WAVES ON A SLOPING SHELF

PRINGLE AND BRINK: HIGH-FREQUENCY INTERNAL WAVES ON A SLOPING SHELF

PRINGLE AND BRINK: HIGH-FREQUENCY INTERNAL WAVES ON A SLOPING SHELF

PRINGLE AND BRINK: HIGH-FREQUENCY INTERNAL WAVES ON A SLOPING SHELF

PRINGLE AND BRINK: HIGH-FREQUENCY INTERNAL WAVES ON A SLOPING SHELF

PRINGLE AND BRINK: HIGH-FREQUENCY INTERNAL WAVES ON A SLOPING SHELF

PRINGLE AND BRINK: HIGH-FREQUENCY INTERNAL WAVES ON A SLOPING SHELF

PRINGLE AND BRINK: HIGH-FREQUENCY INTERNAL WAVES ON A SLOPING SHELF

PRINGLE AND BRINK: HIGH-FREQUENCY INTERNAL WAVES ON A SLOPING SHELF

PRINGLE AND BRINK: HIGH-FREQUENCY INTERNAL WAVES ON A SLOPING SHELF

PRINGLE AND BRINK: HIGH-FREQUENCY INTERNAL WAVES ON A SLOPING SHELF

PRINGLE AND BRINK: HIGH-FREQUENCY INTERNAL WAVES ON A SLOPING SHELF

PRINGLE AND BRINK: HIGH-FREQUENCY INTERNAL WAVES ON A SLOPING SHELF

PRINGLE AND BRINK: HIGH-FREQUENCY INTERNAL WAVES ON A SLOPING SHELF

PRINGLE AND BRINK: HIGH-FREQUENCY INTERNAL WAVES ON A SLOPING SHELF

PRINGLE AND BRINK: HIGH-FREQUENCY INTERNAL WAVES ON A SLOPING SHELF

PRINGLE AND BRINK: HIGH-FREQUENCY INTERNAL WAVES ON A SLOPING SHELF

PRINGLE AND BRINK: HIGH-FREQUENCY INTERNAL WAVES ON A SLOPING SHELF

PRINGLE AND BRINK: HIGH-FREQUENCY INTERNAL WAVES ON A SLOPING SHELF

PRINGLE AND BRINK: HIGH-FREQUENCY INTERNAL WAVES ON A SLOPING SHELF

PRINGLE AND BRINK: HIGH-FREQUENCY INTERNAL WAVES ON A SLOPING SHELF

PRINGLE AND BRINK: HIGH-FREQUENCY INTERNAL WAVES ON A SLOPING SHELF

PRINGLE AND BRINK: HIGH-FREQUENCY INTERNAL WAVES ON A SLOPING SHELF

PRINGLE AND BRINK: HIGH-FREQUENCY INTERNAL WAVES ON A SLOPING SHELF

PRINGLE AND BRINK: HIGH-FREQUENCY INTERNAL WAVES ON A SLOPING SHELF

PRINGLE AND BRINK: HIGH-FREQUENCY INTERNAL WAVES ON A SLOPING SHELF

PRINGLE AND BRINK: HIGH-FREQUENCY INTERNAL WAVES ON A SLOPING SHELF

PRINGLE AND BRINK: HIGH-FREQUENCY INTERNAL WAVES ON A SLOPING SHELF

PRINGLE AND BRINK: HIGH-FREQUENCY INTERNAL WAVES ON A SLOPING SHELF

PRINGLE AND BRINK: HIGH-FREQUENCY INTERNAL WAVES ON A SLOPING SHELF

PRINGLE AND BRINK: HIGH-FREQUENCY INTERNAL WAVES ON A SLOPING SHELF

PRINGLE AND BRINK: HIGH-FREQUENCY INTERNAL WAVES ON A SLOPING SHELF

PRINGLE AND BRINK: HIGH-FREQUENCY INTERNAL WAVES ON A SLOPING SHELF

PRINGLE AND BRINK: HIGH-FREQUENCY INTERNAL WAVES ON A SLOPING SHELF

PRINGLE AND BRINK: HIGH-FREQUENCY INTERNAL WAVES ON A SLOPING SHELF

PRINGLE AND BRINK: HIGH-FREQUENCY INTERNAL WAVES ON A SLOPING SHELF

PRINGLE AND BRINK: HIGH-FREQUENCY INTERNAL WAVES ON A SLOPING SHELF

PRINGLE AND BRINK: HIGH-FREQUENCY INTERNAL WAVES ON A SLOPING SHELF

PRINGLE AND BRINK: HIGH-FREQUENCY INTERNAL WAVES ON A SLOPING SHELF

PRINGLE AND BRINK: HIGH-FREQUENCY INTERNAL WAVES ON A SLOPING SHELF

PRINGLE AND BRINK: HIGH-FREQUENCY INTERNAL WAVES ON A SLOPING SHELF

PRINGLE AND BRINK: HIGH-FREQUENCY INTERNAL WAVES ON A SLOPING SHELF

PRINGLE AND BRINK: HIGH-FREQUENCY INTERNAL WAVES ON A SLOPING SHELF

PRINGLE AND BRINK: HIGH-FREQUENCY INTERNAL WAVES ON A SLOPING SHELF

PRINGLE AND BRINK: HIGH-FREQUENCY INTERNAL WAVES ON A SLOPING SHELF

PRINGLE AND BRINK: HIGH-FREQUENCY INTERNAL WAVES ON A SLOPING SHELF

PRINGLE AND BRINK: HIGH-FREQUENCY INTERNAL WAVES ON A SLOPING SHELF

PRINGLE AND BRINK: HIGH-FREQUENCY INTERNAL WAVES ON A SLOPING SHELF

PRINGLE AND BRINK: HIGH-FREQUENCY INTERNAL WAVES ON A SLOPING SHELF

PRINGLE AND BRINK: HIGH-FREQUENCY INTERNAL WAVES ON A SLOPING SHELF

PRINGLE AND BRINK: HIGH-FREQUENCY INTERNAL WAVES ON A SLOPING SHELF

PRINGLE AND BRINK: HIGH-FREQUENCY INTERNAL WAVES ON A SLOPING SHELF

PRINGLE AND BRINK: HIGH-FREQUENCY INTERNAL WAVES ON A SLOPING SHELF

PRINGLE AND BRINK: HIGH-FREQUENCY INTERNAL WAVES ON A SLOPING SHELF

PRINGLE AND BRINK: HIGH-FREQUENCY INTERNAL WAVES ON A SLOPING SHELF

PRINGLE AND BRINK: HIGH-FREQUENCY INTERNAL WAVES ON A SLOPING SHELF

PRINGLE AND BRINK: HIGH-FREQUENCY INTERNAL WAVES ON A SLOPING SHELF

PRINGLE AND BRINK: HIGH-FREQUENCY INTERNAL WAVES ON A SLOPING SHELF

PRINGLE AND BRINK: HIGH-FREQUENCY INTERNAL WAVES ON A SLOPING SHELF

PRINGLE AND BRINK: HIGH-FREQUENCY INTERNAL WAVES ON A SLOPING SHELF

PRINGLE AND BRINK: HIGH-FREQUENCY INTERNAL WAVES ON A SLOPING SHELF

PRINGLE AND BRINK: HIGH-FREQUENCY INTERNAL WAVES ON A SLOPING SHELF

PRINGLE AND BRINK: HIGH-FREQUENCY INTERNAL WAVES ON A SLOPING SHELF